Intrinsic Ocean–Atmosphere Variability of the Tropical Atlantic Ocean

BOHUA HUANG, PAUL S. SCHOPF, AND J. SHUKLA

Center for Ocean–Land–Atmosphere Studies, Institute of Global Environment and Society, Calverton, Maryland

(Manuscript received 17 March 2003, in final form 8 December 2003)

ABSTRACT

The tropical Atlantic variability is composed of three major patterns of significant importance for variability and predictability of climate in the Atlantic sector. They are the southern tropical Atlantic (STA) pattern with anomalous sea surface temperature (SST) fluctuations expanding from the Angolan coast to the central equatorial ocean, the northern tropical Atlantic (NTA) pattern centered near the northern African coast, and the southern subtropical Atlantic (SSA) pattern in the open subtropical ocean.

Previous studies have suggested that both the regional air–sea coupling and remote forcing from outside the basin may affect the formation of these patterns and their variability. A specially designed global coupled ocean–atmosphere general circulation model, which eliminates air–sea feedback outside the Atlantic, reproduces the major features of these observed patterns realistically. This suggests that these patterns originate from air–sea coupling within the Atlantic Ocean or by the oceanic responses to atmospheric internal forcing, in which there is no anomalous forcing external to the Atlantic Ocean. The effect of the Pacific El Niño–Southern Oscillation (ENSO) seems to modulate their temporal evolution through influencing atmospheric planetary waves propagating into the basin.

One of the problems of the model simulation is that the STA pattern as represented by the SST fluctuations centered at the Angolan coast is weak in the equatorial waveguide. Unlike the observations, the model SST fluctuations around the equator are largely unconnected with the changes in the southeastern part of the ocean. This lack of connection between these two parts of the tropical ocean is related to a model systematic bias of excessive southward shift of the model intertropical convergence zone to around 10°S in boreal spring. In the coupled model, the air–sea feedback forms an artifical ''warm pool'' to the south of the equator extending from the Brazilian coast nearly to the eastern boundary. This warm pool blocks the connection between the fluctuations in the equatorial and the southern part of the ocean. Due to this systematic bias, this model did not simulate the STA pattern adequately.

Several sensitivity experiments have been conducted to further examine the mechanisms of the anomalous SST patterns. The results demonstrate that both the NTA and SSA patterns are mainly associated with the thermodynamic air–sea interactions, while the STA pattern is likely more closely associated with the dynamical response of the equatorial and tropical ocean to the surface wind forcing. Moreover, results from a simulation with a time-independent correction term of the surface heat flux show that the simulated STA mode can be significantly strengthened and have a more realistic spatial structure if the model mean SST errors are reduced.

1. Introduction

There is substantial evidence linking the sea surface temperature anomalies (SSTAs) of the tropical Atlantic Ocean to climate fluctuations in the surrounding regions. The best example may be northeast Brazil, where rainfall anomalies are statistically associated with an Atlantic SSTA ''dipole'' pattern straddling the climatological location of the Atlantic intertropical convergence zone (ITCZ; see e.g., Hastenrath and Heller 1977; Moura and Shukla 1981; Nobre and Shukla 1996). Similar interhemisphere SSTA asymmetry has also been found in composites of major dry and wet years of sub-Saharan Africa (e.g., Lamb 1978a,b; Lough 1986; Folland et al. 1986; Lamb and Peppler 1991).

More recent studies suggest that this dipole configuration reflects the fluctuation of the meridional SST gradient near the equator. Moreover, the gradient changes are usually triggered by the equatorward extensions of the SSTAs originated from either north or south, which are largely unrelated with each other (Houghton and Tourre 1992; Enfield and Mayer 1997; Mehta 1998; Enfield et al. 1999). Therefore, the origination of SSTAs in the northern and the southern tropical oceans may be due to different ocean–atmosphere processes, which is somewhat different than what was previously expected, and needs further investigation.

Figure 1 shows the patterns of the three leading modes of the rotated empirical orthogonal function (REOF) from the observed seasonal mean SSTAs for 1950–98 in the tropical Atlantic. The first mode (Fig. 1a) is char-

Corresponding author address: Dr. Bohua Huang, Center for Ocean–Land–Atmosphere Studies, Institute of Global Environment and Society, No. 302, 4041 Powder Mill Rd., Calverton, MD 20705. E-mail: huangb@cola.iges.org

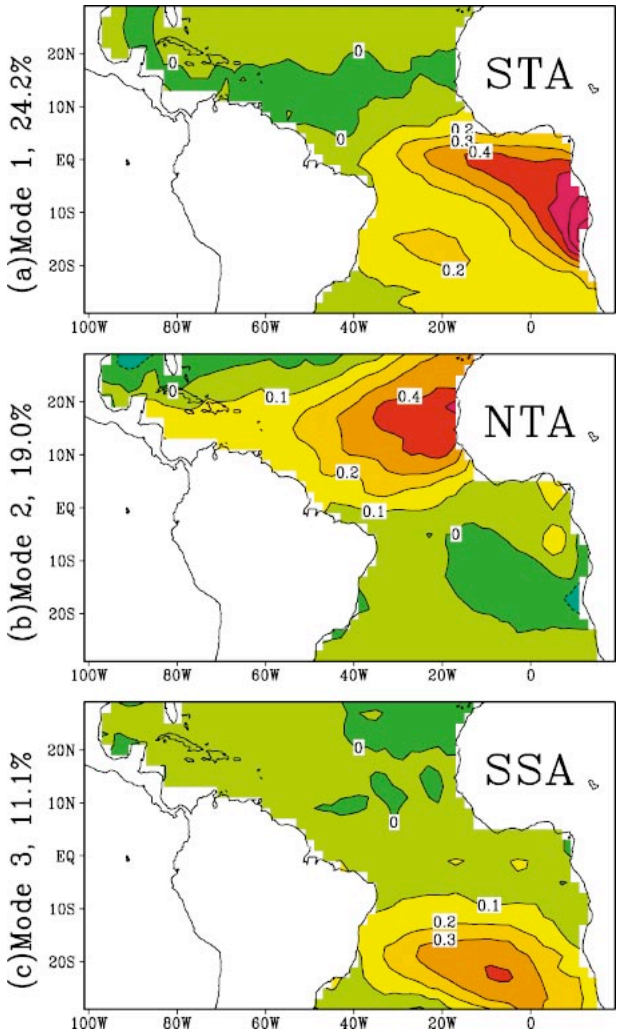

FIG. 1. The spatial patterns of the (a) first, (b) second, and (c) third REOF modes of the seasonal mean SST anomalies for 1950–98. The SST data are from CPC analysis. The contour interval is 0.1°C. The corresponding time series is normalized by its standard deviation.

acterized by SST fluctuations centered near the Angola coast, which extend toward the central equatorial ocean and the Gulf of Guinea, usually referred to as the southern tropical Atlantic (STA) pattern. The second mode (Fig. 1b) presents SST anomalies centered near the African coast in the northern tropical Atlantic Ocean; we refer to it as the northern tropical Atlantic (NTA) pattern. The third REOF mode (Fig. 1c) shows SSTA fluctuations in the open ocean of the subtropical South Atlantic, to be referred to as the southern subtropical Atlantic (SSA) pattern. Both the NTA and STA are well-known patterns of the tropical Atlantic variability. However, not much attention has been paid to the SSA pattern yet, even though it is a part of the dominant SST fluctuation in the subtropical South Atlantic (Venegas et al. 1997). We refer to the variations associated with these three modes as the tropical Atlantic variability (TAV).

Apart from collectively forming an anomalous meridional gradient, there is also evidence that NTA, STA, and SSA patterns all affect the regional climate individually. Year-to-year rainfall fluctuations in the Gulf of Guinea (Wagner and da Silva 1994) and Angola (Hirst and Hastenrath 1983) are associated with the STA fluctuations. The NTA, together with the El Niño–Southern Oscillation (ENSO) cycle in the Pacific, modulates rainfall in the Caribbean–Central America region (Hastenrath 1976, 1984; Enfield 1996; Enfield and Alfaro 1999; Giannini et al. 2000). Robertson and Mechoso (2000) found that the SSA-type SSTA fluctuations are correlated with the interannual variability of the South Atlantic convergence zone (SACZ). These relationships are the major sources of the climate predictability on seasonal to interannual time scales in the tropical Atlantic sector (Hastenrath 1984, 1990; Ward and Folland 1991).

Current hypotheses on the mechanisms that generate the low-frequency interannual ocean–atmosphere processes in the tropical Atlantic region can be classified into two complementary categories. One is regional ocean–atmosphere interaction and the other is the effect of the remotely generated atmospheric or oceanic low-frequency disturbances. It should be pointed out that both of these processes should have relatively high predictability from seasonal to interannual time scales. On the other hand, the atmospheric internal variability, which is less predictable on these time scales, may also affect these SSTA patterns significantly (Dommenget and Latif 2000).

For regional interaction, two air–sea feedback processes have been proposed. Chang et al. (1997) found a decadal oscillation in a hybrid-coupled model of the tropical Atlantic Ocean (an ocean model coupled with a statistical atmosphere). Its positive air–sea feedback involves surface wind speed, evaporation, and SST, usually referred to as the WES feedback (Xie 1999). Zebiak (1993) showed an interannual oscillation in the equatorial Atlantic using an intermediate ocean–atmosphere model. Its structure suggests a positive feedback among the equatorial zonal wind, thermocline tilting, and the SST, similar to that of the Pacific ENSO (Zebiak and Cane 1987). However, both coupled oscillations are not sustainable by themselves within the realistic range of parameters in these simplified models and need to be reinforced by external forcing factors.

Two major remote factors that influence TAV are ENSO and the North Atlantic Oscillation (NAO). There is extensive observational evidence of ENSO effects on TAV. For instance, observations showed that a warm NTA usually appear a few months after the mature phase of the Pacific El Niño (Hastenrath 1984; Curtis and Hastenrath 1995; Harzallah et al. 1996; Enfield and Mayer 1997; Roy and Reason 2001; Czaja et al. 2002). ENSO also tends to lead the SSTA in the Gulf of Guinea for a longer period (Horel et al. 1986; Delecluse et al. 1994; Carton and Huang 1994; Latif and Barnett 1995;

Latif and Grötzner 2000; Jury et al. 2000). Moreover, it has been found that ENSO-induced atmospheric wave trains, which originate from the western Pacific, may affect the South Atlantic SSTA (Mo and Häkkinen 2001). On the other hand, possible extratropical effects, especially those on the NTA from farther north through the NAO, have been documented by some observational and model studies, especially on longer time scales (e.g., Tourre et al. 1999; Tanimoto and Xie 1999; Häkkinen and Mo 2002; Czaja et al. 2002).

Therefore, it is unlikely that we can explain TAV through a single dominant mechanism like the one for ENSO in the tropical Pacific. Instead, we must examine the roles played by each of the potential factors to understand its contribution to the observed SSTA patterns shown in Fig. 1. The identification of their effects using observed data, however, is limited by the substantial overlap between the spatial patterns of the forced and coupled signals in the tropical Atlantic region (e.g., Saravanon and Chang 2000; Chang et al. 2001). This overlap makes it almost impossible to unambiguously determine which process is at work, and different studies seem to get contradictory results. Examining historical data, Czaja et al. (2002) suggested that most NTA peaks in the past few decades could be accounted for by the effects of either the ENSO or NAO and questioned whether regional coupled dynamics over the Atlantic played any role at all. The results from the simplified coupled models (e.g., Chang et al. 1997; Xie 1999), on the other hand, suggested that regionally coupled modes determine the spatial structure and/or time scales of the fluctuations. These models, however, probably overestimated the regional coupling. For instance, statistical SST–wind relationships based on observations are usually used in the hybrid models to determine the atmospheric feedback to the model SST. This kind of relationship sometimes may interpret remotely induced wind disturbances as responses to local SST anomalies. Moreover, these simplified models might neglect some physical mechanisms that are relevant. Thus, further studies based on more realistic models are needed to confirm the results from these simplified models.

In this paper, we analyze the TAV simulated by a coupled ocean–atmosphere general circulation model (CGCM), in which ocean–atmosphere coupling is included only within the Atlantic Ocean between 30°S and 65°N. Outside this region, a climatological SST annual cycle is prescribed. With this regional coupling strategy, one major potential remote forcing factor to the tropical Atlantic, ENSO, is suppressed. Since there is no external SSTA forcing from outside the basin, the regional variability can only be generated by local air–sea coupling and/or oceanic responses to atmospheric internal variations. In this way, we can isolate the local signals from the strong remote ENSO effects and evaluate the TAV development more accurately.

Our results show that this regionally coupled model can reproduce the leading SST patterns shown in Fig. 1 quite realistically. This seems to suggest that these patterns can be produced by air–sea coupling within the Atlantic Ocean or by the oceanic responses to atmospheric internal forcing, in which there is no external SST forcing. The main effect of ENSO and other external forcing may be primarily to modulate the temporal evolution of these modes through influencing atmospheric planetary waves propagating into the basin. Huang et al. (2002a) present a brief account of some preliminary results from this study.

The major problem of the model simulation is that the SSTA in the southeastern tropical Atlantic associated with the STA pattern does not extend into the equatorial waveguide. Unlike the observations, the model SST fluctuations around the equator are largely unconnected with the changes in the southeastern part of the ocean. We find that this lack of connection between these two parts of the tropical ocean is mainly related to a systematic bias of excessive southward shift of the model ITCZ to around 10°S in boreal spring. The air–sea feedback forms an artificial ''warm pool'' to the south of the equator extending from the Brazilian coast nearly to the eastern boundary. This warm pool blocks the connection between the fluctuations in the equatorial and the southern parts of the ocean. Due to this systematic bias, this model did not simulate the tropical dynamical air–sea interactions adequately.

In section 2, the design of the simulation is described, including information on the CGCM and the regional coupling strategy. The simulated mean state and annual cycle are presented in section 3 with emphasis on the ITCZ-related model systematic bias that affects its interannual variability. The interannual SST variability of the coupled model, especially its ability in simulating the leading observational patterns as demonstrated in Fig. 1, is examined in section 4. Results from several additional experiments, which test the sensitivity of the results derived from the regional coupled simulation and further examine the mechanisms of the leading model and observed SST patterns, are presented in section 5. The summary and discussion are given in section 6.

2. Experiment design

The atmospheric and oceanic components of the CGCM are referred to as the AGCM and the OGCM, respectively, hereafter. The AGCM is version 2 of the Center for Ocean–Land–Atmosphere Studies (COLA) AGCM as described in Schneider et al. (2001). It is a global spectral model with a triangular truncation of the spherical harmonics at zonal wavenumber 42, giving roughly a 2.8° latitude × 2.8° longitude resolution in the Tropics. Vertically it is divided into 18 unevenly spaced σ levels with higher resolution in the lower troposphere. There is no sponge layer at the top levels. The model has the same dynamical core as that of the National Center for Atmospheric Research (NCAR)

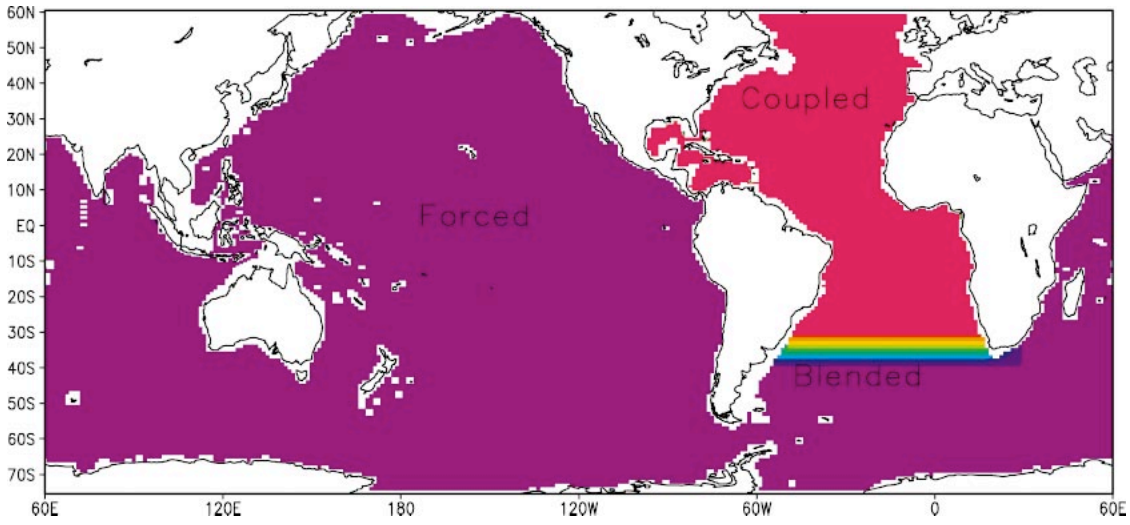

FIG. 2. The regional coupling strategy over the oceanic domain. The fully coupled region is red. The rest of the oceanic region where the OGCM and the AGCM are forced with data is in purple. The zonal belt over the South Atlantic with changing colors is the blending zone.

Community Climate Model version 3.0 (CCM3) and a semi-Lagrangian moisture transport scheme.

The AGCM's physical parameterizations include solar (Lacis and Hansen 1974; Davies 1982) and terrestrial (Harshvardhan et al. 1987) radiation schemes. The deep convection is parameterized by the relaxed Arakawa–Schubert scheme (Moorthi and Suarez 1992), implemented in this model as in DeWitt (1996). The shallow convection follows the scheme of Tiedke (1984) and the convective cloud fraction follows the scheme used in the CCM3 (Kiehl et al. 1994). The Mellor and Yamada (1982) level 2.0 closure scheme is used for turbulent transport of heat, momentum, and moisture. There is also a parameterization of gravity wave drag (Palmer et al. 1986).

The OGCM is a nonlinear reduced-gravity model of quasi-isopycnal layers, which is described in more detail in Schopf and Loughe (1995) and Yu and Schopf (1997). The model domain is the World Ocean within 70°S–65°N. It has 14 layers in the vertical and a horizontal resolution of 1° latitude × 1.25° longitude while the meridional resolution is increased to 0.5° within 10°S–10°N to resolve the equatorial waves more accurately. The first model layer represents the well-mixed surface layer. The entrainment at its base is calculated through a balance of wind stirring, release of mean kinetic energy due to shear at the base of the layer, dissipation, and the increase in potential energy due to mixing, as set forth in Niiler and Kraus (1977). The internal shear-induced vertical mixing and diffusion are based on the Pacanowski and Philander's (1981) Richardson-number-dependent scheme. There is also a convective overturning adjustment when the water column becomes statically unstable. Horizontal mixing is accomplished though a modified Shapiro (1970) filter, which is applied to the mass, temperature, and momentum fields.

Although both the OGCM and AGCM are global, they are fully coupled only in the Atlantic Ocean within 30°S–65°N for this study. Within the coupled region (Fig. 2, red regions), the surface fluxes of heat, freshwater, and momentum at the sea surface simulated by the AGCM are provided to the OGCM at daily intervals. The OGCM-simulated SST over the Atlantic for the same interval is then supplied to the AGCM. Over the uncoupled portion of the global domain (Fig. 2, purple regions), the climatological monthly SST calculated from the U.S. Climate Prediction Center's (CPC) SST data for 1950–98 (Smith et al. 1996) is prescribed for the AGCM. Since the OGCM is a global model, wind stress, heat, and freshwater fluxes are also required over the uncoupled region. The climatological monthly surface wind stress is prescribed from the National Centers for Environmental Prediction (NCEP) reanalysis (Kalnay et al. 1996). The net surface heat flux into the OGCM over the uncoupled portion of the global domain is given by the AGCM flux plus a relaxation term to the prescribed SST with a rate of 30 W m^{-2} per degree of the difference between the prescribed and model-produced SST. The freshwater flux is given from the AGCM output. A 10° wide zone in the South Atlantic Ocean within 30°–40°S is used to blend the coupled and uncoupled portions of the domain.

The ocean and atmosphere states used to initiate the coupled model are separately derived from long-term uncoupled simulations of these two component models. From this initial ocean–atmosphere state, the coupled run has been carried out for 200 yr. The output from the last 110 yr is used in this analysis.

3. Mean state and annual cycle

Before examining the interannual variability in the tropical Atlantic from the simulation, we first compare its mean state and annual cycle with observations. The

mean states and annual cycles produced by coupled models for the tropical Pacific have been critically examined by many studies (e.g., Neelin et al. 1992; Mechoso et al. 1995; Schneider et al. 1997; Meehl and Arblaster 1998). However, as far as we know, there have been no comparable examinations for the coupled tropical Atlantic simulations. We believe such an examination is relevant here because, as we have stated in the introduction and will show later on, some problems in the interannual variability simulated by this particular model are closely related to the systematic errors in the mean field. Moreover, since the annual cycle is the dominant signal in the tropical Atlantic, a prerequisite of a successful model simulation of the regional climate variations should be that it reproduces the observed annual component.

The model reproduces the major features of observed SST and surface wind stress (Figs. 3a,b) and net heat flux into the ocean (Figs. 3c,d), though with noticeable differences in some areas. For example, the observed net surface heat flux into the ocean is around 60–80 W m^{-2} near the African coast around 10°–20°N (Fig. 3d), based on the estimate of the Coupled Ocean–Atmosphere Data Set (COADS) climatology (da Silva et al. 1994), while the simulated flux is nearly zero there (Fig. 3b). The reason is that the model has more cloudy skies in this region so that less solar radiative flux reaches the sea surface. The simulated regional mean SST, however, does not show a corresponding error (Fig. 3e). Actually, the model SST is slightly warmer than the observed because the weak alongshore winds suppress local upwelling.

There is another model mean bias that has more serious consequences to its seasonal cycle and interannual variability. In the model, the warm water residing in the western ocean with mean temperature higher than 27°C penetrates toward the eastern boundary at around 5°–15°S (Fig. 3a). This penetration largely cuts off the link between the cold water in the eastern equatorial ocean and the coastal region farther to the south, which collectively forms the observed cold tongue (Figs. 3a,c). As a result, the simulation shows a positive SST error, larger than 3°C at its center near the eastern boundary around 15°S, that extends northwestward to the equator (Fig. 3e). This SST error reflects the climate drift of the coupled system, with the southeast trade winds weaker than observed from the equator to around 15°S, located mostly to the north and west of the SST errors (Fig. 3e). The simulated mean precipitation also shows a strong center of precipitation (7 mm day^{-1}) over the western part of the warm water belt around 5°–10°S, which has no correspondence to observations.

This systematic error in the model's mean fields is closely connected to its annual cycle. In fact, the model and observations have a different latitudinal range of the seasonal migration of the ITCZ, as measured by the climatological monthly mean precipitation over the Atlantic Ocean (Fig. 4). The observations (panels in the left-hand column) show an annual ITCZ migration from near the equator in April (Fig. 4c) to around 10°N in August (Fig. 4g) and October (Fig. 4i). The model ITCZ (panels in the right-hand column), on the other hand, is located between 5° and 10°S from February (Fig. 4b) to June (Fig. 4f) when the model SST is warmest in this area. In June, a separate rainfall belt reappears in the model to the north of the equator over the Atlantic Ocean, which is then enhanced and moves northward to reproduce the observed location at 10°N from August (Fig. 4h) to October (Fig. 4j). During this period, the southern branch of the rainfall is weakened but persists near the coast of South America (Figs. 4h,j).

Scatterometer observations show July surface convergence at about the same location as the model's southern rainfall belt (Liu and Xie 2002). This surface convergence is attributed to shallow dry convection induced by weakening surface meridional winds from warmer water to the south advecting to the equatorial cold tongue because of vertical stability changes in the atmospheric boundary layer over warmer and colder waters. However, in the AGCM, this convergence seems to trigger deeper convection, and in the coupled model the resulting feedback changes the SST. As a result, the model produces a strong southern precipitation belt in boreal spring and early summer, which is not observed in either the CPC analysis or the scatterometer data (Liu and Xie 2002). This model rainfall pattern is similar to the migrating, and sometimes double, ITCZ feature of some coupled models in the tropical Pacific Ocean documented by Mechoso et al. (1995) and Meehl and Arblaster (1998). As we have stated above, it probably originates from inaccuracies in the parameterization of the convection in the Tropics.

Williamson et al. (1995) demonstrated that, given the prescribed SST distribution, the simulation of the ITCZ is sensitive to the resolution of the AGCM. Analyzing uncoupled OGCM and coupled GCM simulations in the tropical Pacific Ocean, Huang and Schneider (1995) and Schneider et al. (1997) found that weak alongshore winds produced by an AGCM suppress upwelling near the South American coast and cause warmer SST errors near the coast. Errors in the wind direction and speed near the Angolan coast may cause a similar problem in the simulation of the tropical Atlantic Ocean (Fig. 3e). There are other potential sources that may cause or amplify the errors in the coupled model. Mechoso et al. (1995) pointed out that the effects of stratus clouds, evaporation–wind feedback, and oceanic coastal processes might also play some roles here.

Even though there is a problem in simulating the ITCZ location, the model still reproduces the observed annual strengthening of the easterlies in the western Atlantic starting in June and peaking in September (Figs. 5a,b). This wind change corresponds to an enhancement and westward expansion of the cold water during the same period (Figs. 5c,d). The warming of the SST in the eastern ocean during boreal spring is also well re-

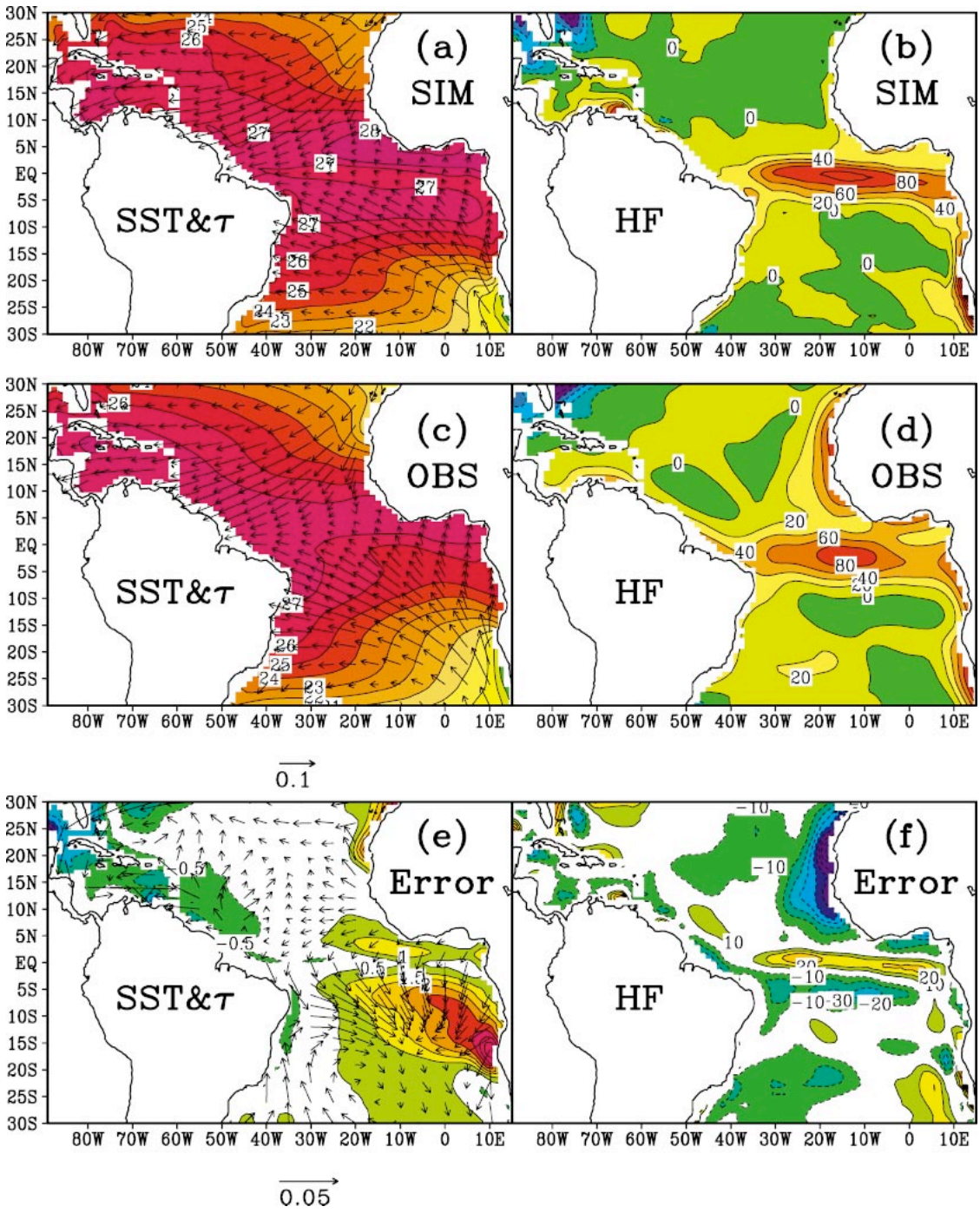

FIG. 3. The annual mean state of the (a) SST and surface wind stress and (b) surface heat flux over the tropical Atlantic Ocean from the simulation. (c), (d) The same variables from the observations. (e) The model error for the SST and surface wind stress and (f) for the surface heat flux. The contour intervals are 1°C for SST in (a) and (c), and 0.5°C for SST errors in (e). The contour intervals are 20 W m^{-2} for the heat fluxes in (b) and (d), and 10 W m^{-2} for the heat flux error in (f). The arrow under (c) is 0.1 N m^{-2}, representing the unit vector in (a) and (c). The arrow under (e) is 0.05 N m^{-2}.

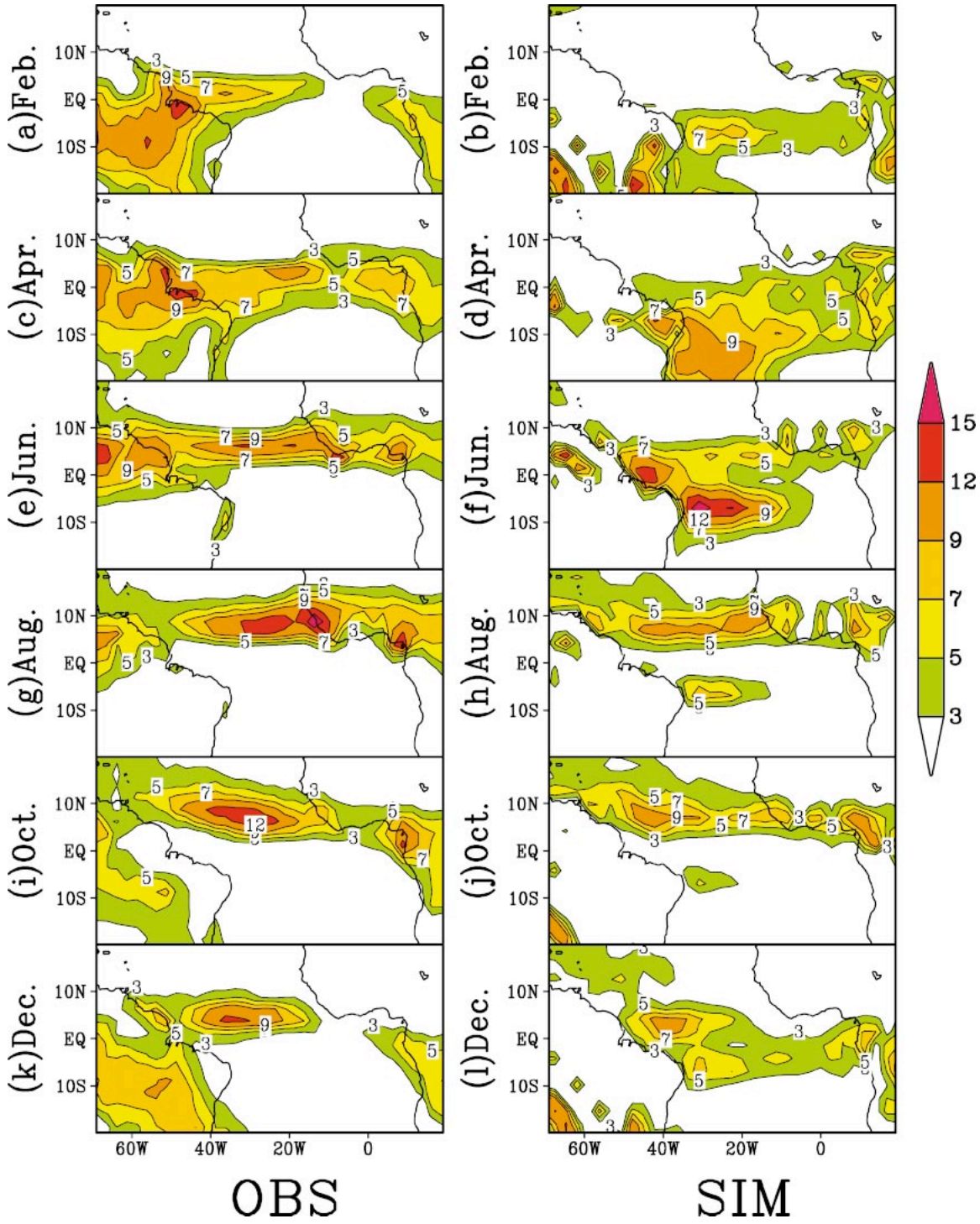

FIG. 4. Climatological monthly precipitation over the tropical Atlantic region from the CPC analysis and the simulation. The fields are presented every other month from Feb to Dec. The observations are given in the left-hand panels; the corresponding model results in the right-hand panels. For each panel, the contour intervals are 3, 5, 7, 9, 12, and 15 mm day^{-1}.

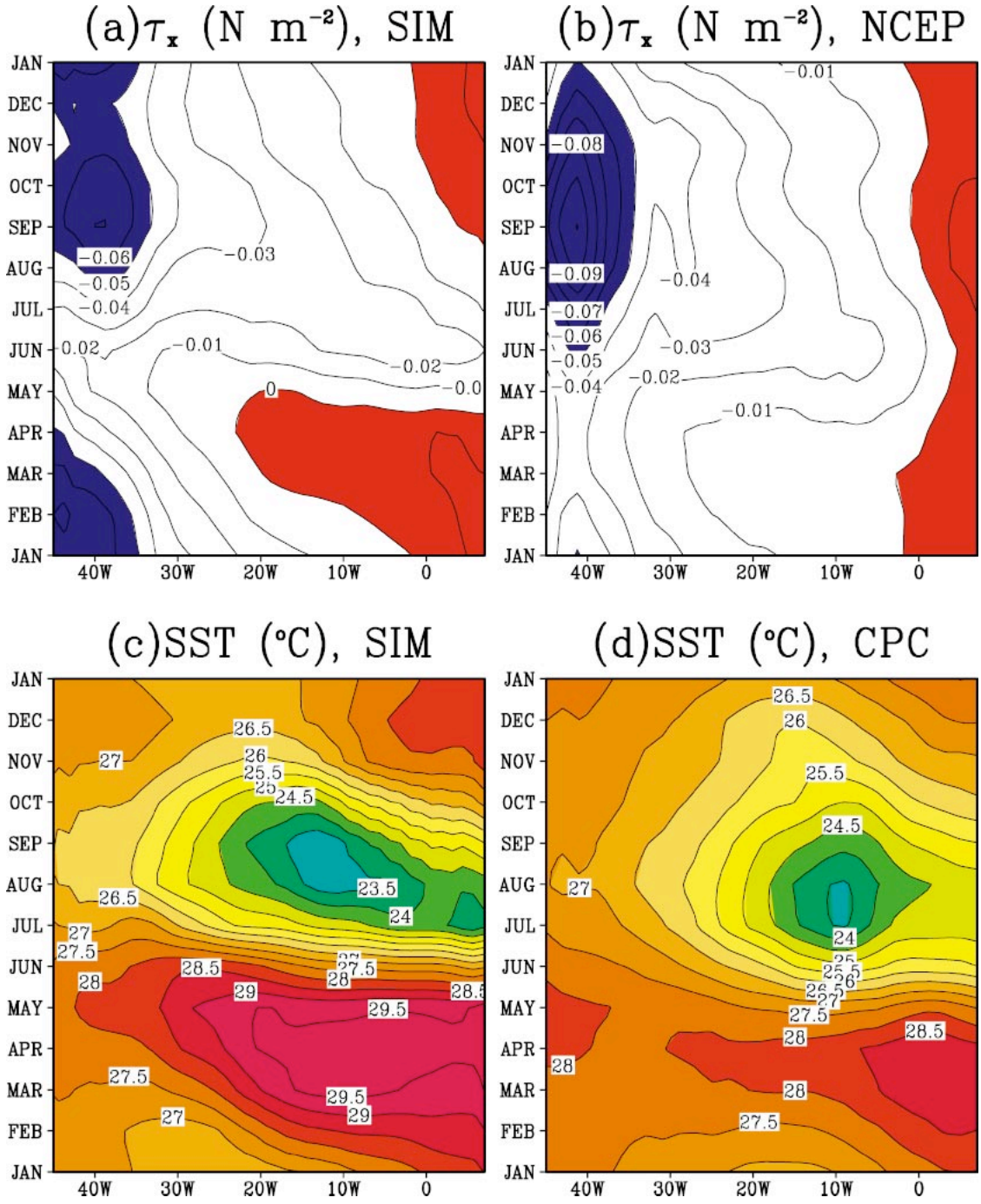

FIG. 5. Time–longitude sections of the climatological monthly wind stress and SST averaged within 2°S–2°N over the Atlantic basin. The top two panels are wind stress from (a) the simulation and (b) the NCEP–NCAR reanalysis. The bottom two panels are SST from (c) the simulation and (d) the CPC analysis. The contour interval is 0.01 N m^{-2} for the stress and 0.5°C for SST.

produced. The simulated warming and cooling are about 1°C larger than the observations. The excessive warming in boreal spring is due to the weaker easterlies over the central and eastern ocean because the strong southern ITCZ blocks the southeast trades from reaching the equatorial ocean (Figs. 5a,b). Considering that both the model zonal and meridional wind stresses are weaker than the observations in boreal summer, the colder model SST suggests greater sensitivity to changes of the surface stress, which is probably related to the model vertical mixing within the ocean. West of 40°W, there is a secondary model easterly wind peak in February

(Fig. 5a), which has no counterpart in observations. This is caused by the northeast trades penetrating to the equator, associated with the southern bias of the ITCZ. This wind error, however, does not cause a significant SST change in the eastern ocean.

The model's annual harmonics of surface wind stress, heat flux, and the SST are largely consistent with observations in the tropical and subtropical region. In general, the amplitude of the model SST annual wave is larger than observed while there is no such tendency in the winds and heat flux. This suggests that the model mixed layer is more sensitive to the surface forcing changes than is the observed one. The model annual cycle is weak near the eastern part of the tropical ocean south of the equator at 5°–15°S because the warm SST bias limits the expansion of cold water from the eastern boundary.

Overall, the simulation produces qualitatively realistic mean fields of the SST, the surface wind stress, and the net surface heat flux in the fully coupled tropical Atlantic region. The model also simulates a realistic annual cycle with the amplitude and phase largely comparable to the observations in most of the region. However, the model systematic error in the southern tropical ocean has a significant effect on the patterns of the tropical Atlantic interannual variability, as we will see in the next section.

4. Major interannual SSTA modes

The observed standard deviation (STD) for SSTAs, based on the 49-yr CPC data, shows three major regions with standard deviation larger than 0.4°C (Fig. 6a). These are the tropical North Atlantic and South Atlantic regions, both centered at the African coasts, as well as the subtropical South Atlantic in the open ocean. Significant variations (STD $>$ 0.5°C) extend from the eastern boundary of the South Atlantic around 15°S to the central equatorial ocean, suggesting a strong connection between the variations in the southeast and those within the equatorial waveguide. This STD distribution is consistent with the three leading REOF modes characterizing the southern tropical Atlantic (STA), the northern tropical Atlantic (NTA), and the southern subtropical Atlantic (SSA) patterns (Fig. 1). On the other hand, the lower SSTA STD (say, $<$0.3°C) generally resides in the region with relatively higher mean SST (say, $>$28°C; see the mean SST fields from the model and the observations in Figs. 3a and 3c).

The coupled model qualitatively simulates the three observed centers of variability (Figs. 6a,b). The magnitude of the model STD is generally a little higher than observed, as in the case of the annual cycle. A major discrepancy between the model and observations is a zonal belt of low STD centered at 10°S extending eastward. It is clearly associated with the higher model mean SST in this region. Its effect is the separation of the high STD region near the southeastern boundary into two parts: one around the equator and the other between 10° and 20°S. In particular, the model equatorial SSTA variability near the eastern coast is higher than observed. Also like the annual cycle, the STD of model zonal wind stress anomalies is generally smaller than observed (not shown).

Our REOF analysis of the model SSTA shows that the leading SST patterns shown in Fig. 1 can be reproduced quite realistically by the first three REOF modes of the SST anomalies produced by this regionally coupled model (Fig. 7). To be directly comparable with the observed STA, NTA, and SSA patterns shown in Fig. 1, the first three simulated REOF modes are presented in Fig. 7 in the order from small to large explained total variances. We find that the first (Fig. 7c) and second REOF modes (Fig. 7b) show spatial patterns very similar to the observed SSA (Fig. 1c) and NTA patterns (Fig. 1b). These two model modes explain a significant amount of the total variance (14.6% and 12.2%, respectively) and their magnitudes are comparable to their observed counterparts (Figs. 1b,c). This suggests that these patterns can be produced by air–sea coupling within the Atlantic Ocean or by the oceanic responses to atmospheric internal forcing, in which there is no external SST forcing. Moreover, these two patterns are very similar to the leading REOF modes of the annually averaged SSTA from several globally coupled GCM simulations shown in Dommenget and Latif (2000). The patterns of the two leading EOF modes of the simulated SSTA demonstrated by Cabosnarvaez et al. (2002) from the ECHAM4–Ocean and Isopycnal Coordinates (OPYC3) coupled model (Roeckner et al. 1995) are also somewhat similar.

The spatial structure of the third model REOF mode shows a center of variability near the eastern boundary between 10° and 20°S extending toward the west-northwest (Fig. 7a). Since the location of the center is the same as that in the observed STA pattern (Fig. 1a), we refer to this mode as the model STA pattern. However, it should be noted that the model STA pattern is different from the observed one in the equatorial region. Unlike the observations, the model variations are more confined to the south of 10°S. Moreover, the model STA is much weaker than the observed (8.6% versus 24% of the total variances). One of the potential reasons for the weak model STA mode in the equatorial region is that ENSO, which may remotely generate equatorial wind fluctuations in the Atlantic sector, is eliminated in the model.

The distribution of variances among the three leading REOF modes in the model is apparently different from that of the observations, which reflect different influences of various physical processes in the model and the simulations. Although the observations are dominated by the STA pattern centered at the eastern boundary and the equatorial ocean, the model shows stronger variations away from the equator, in the southern and northern tropical and subtropical regions. In a composite analysis of the SST anomalous events peaking at dif-

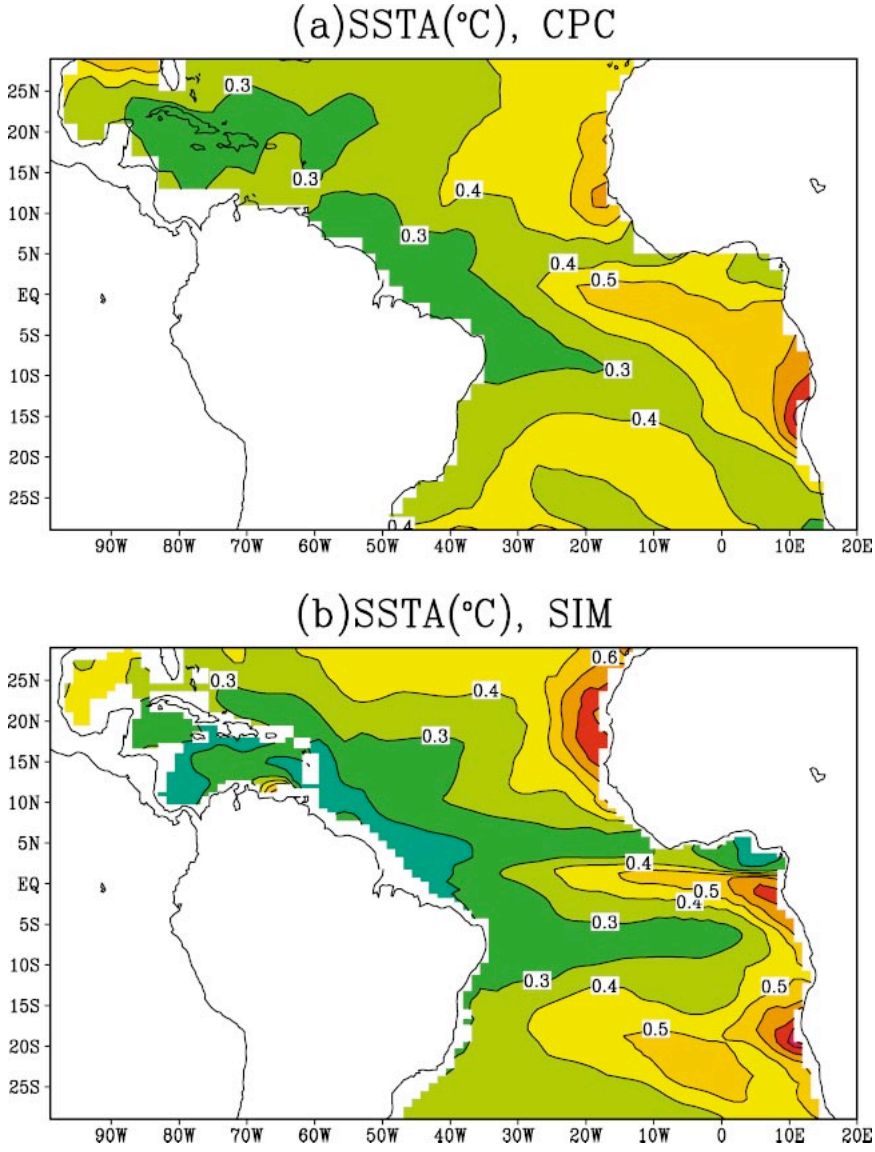

FIG. 6. The spatial structure of the standard deviation of the seasonal mean SST anomalies from (a) the CPC analysis for 1950–98 and (b) the 110-yr simulation of the regional CGCM. The contour interval is 0.1°C. The SST anomalies are seasonally averaged data.

ferent seasons, Huang and Shukla (2003, manuscript submitted to *J. Climate,* hereafter HS) show that, in both observations and this regional coupled model, the SST fluctuations with the SSA and NTA patterns are associated with trade wind fluctuations, which are sometimes caused by the extratropical atmospheric disturbances to subtropical anticyclones. The higher percentages of the variances explained by the model SSA and NTA imply a stronger extratropical atmospheric influence on the tropical ocean in the simulation. As we will see next, another reason for the relatively large percentages of the total variance explained by these two modes is that the tropical process represented by the observed STA pattern is not adequately simulated by the model.

The three leading observed REOF modes (Fig. 1), which explain about 54.3% of the total variance, seem to be adequate in representing the major observed signals. They are also well separated from the higher modes by a gap in the explained variance. These features suggest a logical truncation after the third mode in considering major patterns of the variability in this region. (The fourth and fifth observed modes, e.g., explain 6.5% and 6.2% of the total variance, respectively.) On the other hand, the first three simulated REOF modes only explain 35.4% of the total variance. In fact, the percentages of the total variances explained by the fourth and fifth modes (8.2% and 8.0%) are comparable to that of the third mode. Therefore, in considering the major

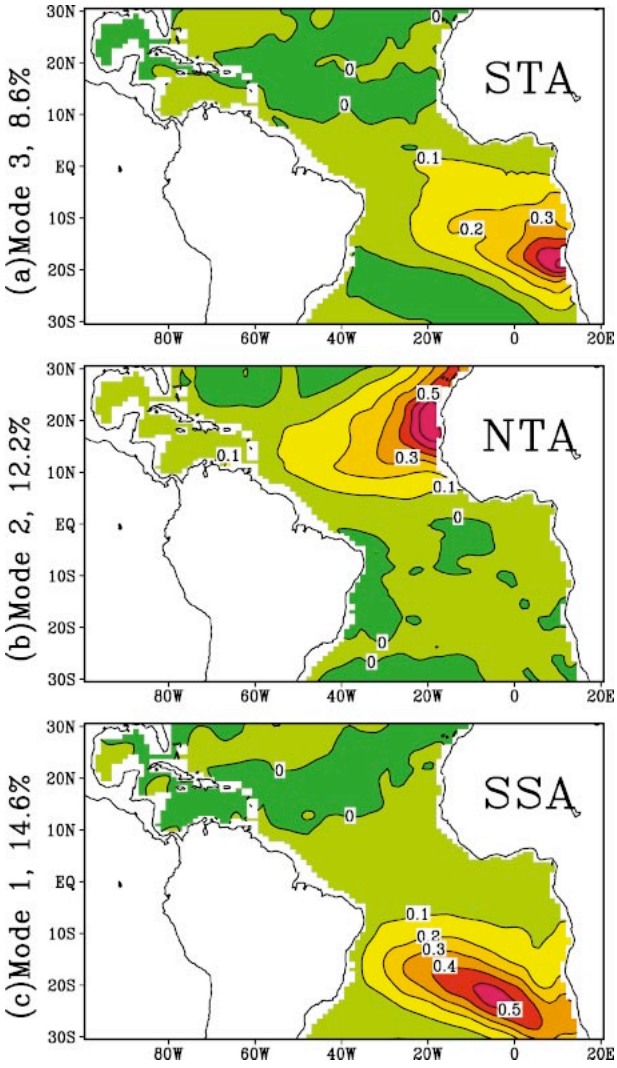

FIG. 7. The spatial patterns of the (a) third, (b) second, and (c) first REOF modes of the seasonal mean SST anomalies from the 110-yr regional coupled GCM simulation. The contour interval is 0.1°C. The corresponding time series of each mode is normalized by its standard deviation.

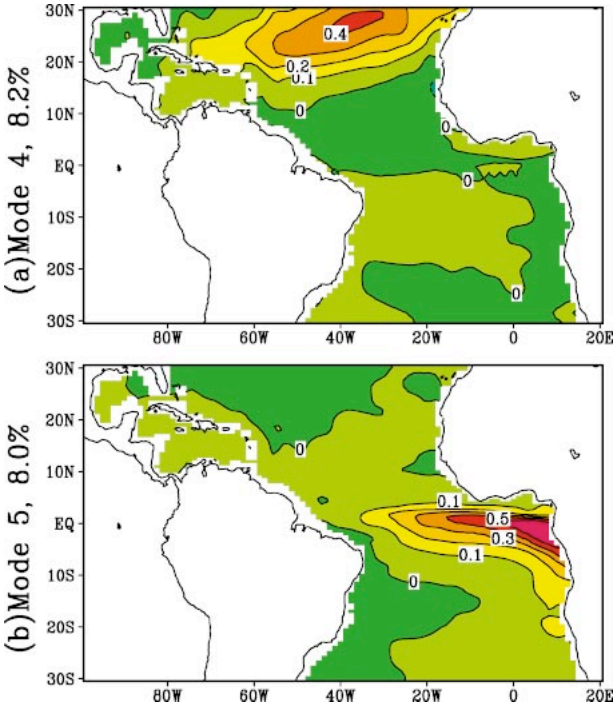

FIG. 8. The spatial patterns of the (a) fourth and (b) fifth REOF modes of the seasonal mean SST anomalies from the 110-yr regional coupled GCM simulation. The contour interval is 0.1°C. The corresponding time series of each mode is normalized by its standard deviation.

variations, a truncation after the fifth mode seems to be more reasonable in the model. This increases the percentage of explained total variance to 51.6% and forms a more natural gap to the higher modes. The sixth model mode explains about 5% of the total variance.

The fourth model REOF mode (Fig. 8a) depicts subtropical SSTA fluctuations centered near 30°N in the central part of the North Atlantic. The spatial structure of this mode is similar to one of the higher REOF modes of the SSTA from the observations (not shown) though its observed counterpart explains a smaller amount of the total variance. Conducting a season-by-season REOF analysis of both the model and observed SST anomalies, HS find that, unlike the NTA mode, which is strongest in boreal winter and spring (Nobre and Shukla 1996), the pattern represented by the fourth mode is more likely to be stronger in boreal summer and seems to be associated with the tropical extension of the midlatitude SST anomalies identified by Czaja and Frankignoul (2002) as the ''North Atlantic Horseshoe'' pattern. The strengthening of this mode in the simulation seems to be further evidence of the intense model extratropical atmospheric fluctuation. The fifth mode (Fig. 8b), on the other hand, represents an equatorial variability largely confined within the equatorial waveguide (7°S–7°N). Its spatial structure and relationship to equatorial zonal wind fluctuations are similar to those in the equatorial oscillation produced by Zebiak (1993) using an intermediate coupled ocean–atmosphere model and to the equatorial portion of the observed STA pattern (Fig. 1a).

The necessity to include more modes to adequately describe the simulated SST interannual variability is implied in the higher effective number of spatial degrees of freedom (ESDOF; Bretherton et al. 1999) of the model data than that of the observations. The ESDOF can be estimated for the observed and the simulated seasonal mean SST anomalies of the tropical Atlantic basin using two measures. Both match data to a chi-squared distribution, one using the mean and variance of the time series of the spatially integrated squared anomalies and the other using the squared eigenvalues of a covariance matrix. For normally distributed samples, these two measures are equivalent to each other. In our case, both

measures give quite consistent ESDOF estimates of 5.56 and 5.47 for the observational data. The estimates from the simulated data, on the other hand, give the values of 8.28 and 11.46, respectively, with the eigenvalue approach giving a higher estimate. This suggests that the leading model principal components have larger kurtosis than a normal distribution does (Bretherton et al. 1999).

Overall, the model's effective number of the spatial degrees of freedom is apparently larger than that of the observations. It is possible that the higher spatial resolution of the ocean model allows more active small-scale fluctuations. However, the major reason is likely that the model cannot activate some major dominant modes to the strength shown in the observations, as we have seen in the STA case. The situation is probably not that unusual for numerical models. A similar lack of concentration of the active modes has been shown by Fraedrich et al. (1995) for an AGCM simulation. On the other hand, we should point out that the ESDOF could be underestimated in the observed SST analysis. The analyzed SST fields in the tropical Atlantic Ocean are constructed by optimally fitting in situ measurements for 1950–81 to 23 prescribed spatial patterns from the EOF modes of the more accurate analyses for 1982–93 (Smith et al. 1996). The projection of the sparse observations onto the given patterns during the earlier period may severely influence the ESDOF.

It is interesting to note that the pattern of the third model REOF mode (Fig. 7a) is similar to that of the observed STA (Fig. 1a) near the southeastern boundary while the fifth mode (Fig. 8b) shows some characteristics of this observed mode near the equator. Unlike the observations, however, the simulated SST anomalies fluctuate largely independently between these two regions. We believe that this reflects a fundamental difference between the simulation and the observations. Hirst and Hastenrath (1983) suggested that the observed STA pattern is associated with air–sea interactions and oceanic waves in the equatorial waveguide and is sensitive to the equatorial wind in the western and central Atlantic. Our results suggest that the coupled model does not simulate the connection between the equatorial and the southeastern regions well. We suspect that this inadequacy is related to the warm mean SST bias to the south of the equator as described in the last section and the fact that in the coupled model the ITCZ has two preferred locations. As in the annual cycle, this zone largely cuts off the link between the interannual fluctuations near the Angolan coast and those within the equatorial waveguide, which splits them into two separate modes as shown in the leading REOF modes and the STD distribution (Fig. 6b). We noted that the spatial structures similar to the observed STA pattern (Fig. 1) are not among the first two leading EOF or REOF modes of the tropical Atlantic SST anomalies as simulated by some other CGCMs (e.g., Dommenget and Latif 2000; Cabosnarvaez et al. 2002). It is possible that model errors have a similar influence on the interannual modes in these simulations.

It is also possible that, due to the influence of equatorial ocean dynamics, the STA mode fluctuates on shorter time scales than for the two other patterns. To examine the influences of the higher-frequency signals, we have conducted the REOF analysis using monthly mean values of both observed and simulated SST anomalies. For the simulation, the spatial patterns of the five leading modes are largely unchanged. Compared to the seasonally averaged data, there is a small reduction of the explained total variance by each of the leading modes in the monthly case, but the fifth mode remains a logical truncation point. The observed spatial patterns of the three leading modes are also largely unchanged. On the other hand, we notice that the percentage of the total variance explained by the fourth mode is significantly increased. The pattern of the fourth mode (not shown) is dominated by SST anomalies in the central equatorial and southern tropical Atlantic, which represents the subsequent northwestward propagation of the STA SST anomalies after the peak phase shown in Fig. 1a. In fact, the time series of the observed fourth mode shows a maximum correlation of 0.34 to that of the STA pattern at a lag of 4 months. We found no counterpart to the observed fourth mode in the model, possibly because the model STA is weaker and less persistent. Moreover, our examination does not show any significant lagged connection between the model's third (Fig. 7a) and fifth (Fig. 8b) modes in either the monthly or seasonal data, as was shown in the observational case. Overall, the higher-frequency fluctuations do not change the basic patterns of the SST anomalies significantly for the model and the observations.

The time series of the model NTA, SSA, and STA patterns show similar statistical features with their observed counterparts. The model STA pattern is represented by the third REOF mode here. Power spectra of the STA and NTA from both the model (Figs. 9a,b) and the observations (Figs. 9d,e) largely follow red noise distributions consistent with what Dommenget and Latif (2000) have shown. All four of these time series show one-season-lagged autocorrelation around 0.6. Both observed and model STA have local maxima at periods about 1.5 yr (Figs. 9a,d). For the NTA pattern, the observations show local peaks of variability at periods of 2.5, 4, and 10 yr. The model shows local maxima at 1.5-, 2-, and 4-yr periods and a much weaker peak at around 8–9-yr periods. However, it is possible that none of these peaks are significantly distinguishable from the spectra of the red noise.

Compared with the STA and NTA patterns, both model and observed SSA spectra are flatter (Figs. 9c,f). Correspondingly, their autocorrelations at one season's lag are also smaller, at 0.30 for the model and 0.46 for observations. For periods longer than 1 yr, the observed spectrum has peaks with periods at around 5 and 16 yr. The decadal period is similar to what Venegas et al.

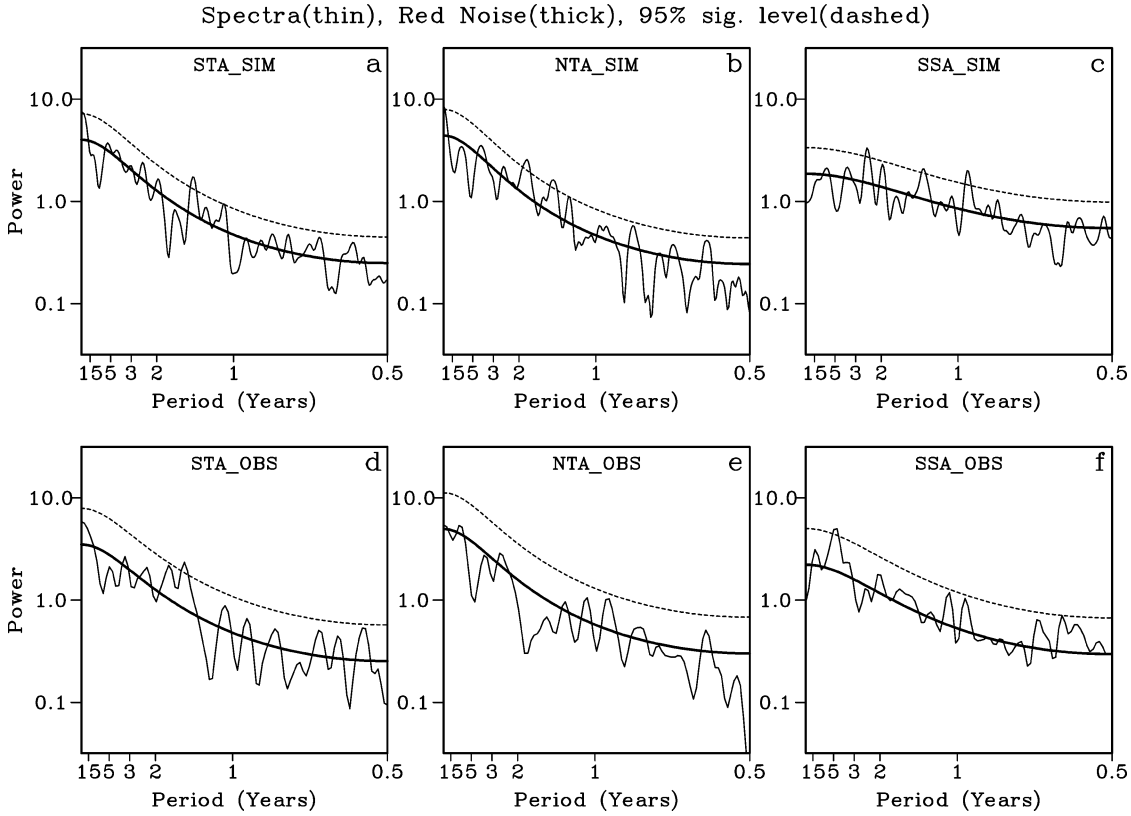

FIG. 9. Power spectra of the time series of the (a) STA, (b) NTA, and (c) SSA modes from the seasonal data of the 110-yr simulation. (d)–(f) The corresponding power spectra of these modes from the 49-yr (1950–98) observational data.

(1997) found in their first singular value decomposition (SVD) mode between SST and sea level pressure (SLP) in the South Atlantic. The model, on the other hand, fluctuates mostly on interannual time scales. There are three local maxima around 2.5, 1.5, and slightly less than 1 yr in its spectrum. It is interesting to note that there is a lack of lower-frequency fluctuations in the model SSA in comparison with the observed one. A possible explanation is that there is no air–sea feedback south of 30°S and therefore the lower-frequency signals of the model SSA are suppressed. The spectrum of the time series for the fourth REOF mode of the simulated SST anomalies also follows a red noise distribution (not shown). Its autocorrelation with one-season lag is 0.44, lower than that of the NTA mode. The time series of the model fifth REOF mode, on the other hand, is closer to a white noise distribution in its spectrum (not shown).

Each of these modes has a significant seasonal dependence, as shown by separate REOF analysis for each season reported in HS. The observed NTA is dominant in boreal spring (March–May), as pointed out by Nobre and Shukla (1996). Moreover, the center of the variations near the African coast migrates from 20°–30°N in boreal summer and fall to 10°–20°N in winter and spring. As we have mentioned before, the center of SST anomalies in the north during the summer is associated with the ''North Atlantic Horseshoe'' pattern shown in Czaja and Frankignoul (2002). The model NTA mode is not as strongly enhanced in boreal spring as in the observations. However, it does reproduce the observed southward shift of the action center from autumn to winter as well as the connection with the North Atlantic horseshoe pattern. On the other hand, the model SSA is dominant in austral summer (December–February), which is consistent with the observations. Whereas for the STA centered near the Angolan coast, the observed mode is dominant in boreal summer (June–August), while the model mode is strongest in boreal fall (September–October). The equatorial SSTA fluctuations in the eastern Atlantic Ocean as shown in Fig. 8b also get stronger in boreal summer and fall in the model. This SSTA variability is strictly trapped within 10°S–10°N and separated from the center of the STA around 15°S near the African coast. A composite analysis of the major events associated with this equatorial mode shows that the evolution of the ocean–atmospheric anomalies is largely within the equatorial waveguide (HS).

5. Sensitivity experiments

We have conducted several sensitivity experiments to further study the mechanisms of the major patterns of

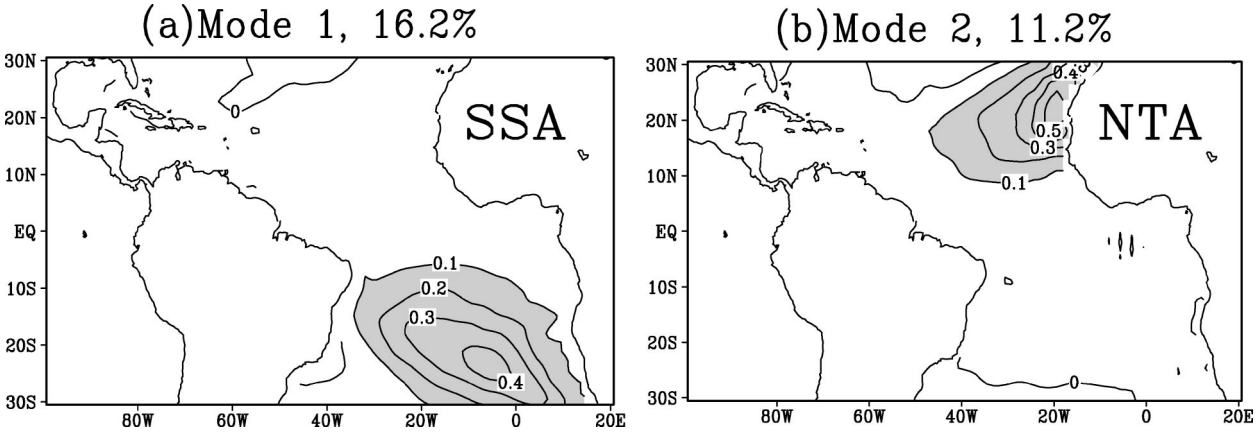

FIG. 10. The spatial patterns of the (a) first and (b) second REOF modes of the seasonal mean SST anomalies from the thermal experiment. The contour interval is 0.1°C. Regions with SST anomalies larger than 0.1°C are darkly shaded and those less than −0.1°C are lightly shaded. The corresponding time series of each mode is normalized by its standard deviation.

the tropical Atlantic SST anomalies. We also examined the effects of the systematic errors and the regional coupling procedure in the model. The sensitivity runs to be reported generally last for several decades to a hundred years. In analyzing the results of these experiments, we concentrated on the leading REOF modes of the SST anomalies. As described in the last section, the truncation of modes is based on the gap in the explained total variance. From now on, we will refer to the 110-yr simulation of the regional coupled model over the Atlantic Ocean from 30°S to 60°N discussed in the previous sections as the ''control'' run.

In one experiment, we eliminated the momentum exchange between the AGCM and the OGCM of the coupled model over the Atlantic Ocean within 30°S–60°N by replacing the surface wind stress forcing to the OGCM there with a monthly climatology derived from the control run. In this case, the two components of the model are dynamically uncoupled but still interact with each other thermodynamically because the AGCM-produced surface heat flux forces the OGCM and the OGCM-produced SST forces the AGCM. This experiment examines the effects of the thermodynamic interactions between the ocean and the atmosphere on the major tropical Atlantic SST patterns and is referred to as the thermal simulation.

From a 100-yr thermal simulation, it is found that the SST anomalies reproduce both the SSA and the NTA patterns quite realistically (Figs. 10a,b), which suggests that these patterns are formed primarily by the effect of the surface heat flux and the thermodynamic air–sea interaction. The effects of the dynamical air–sea interactions are secondary. It is somewhat surprising that the NTA pattern (Fig. 10b) can be simulated in this heat-flux-only case because the observed NTA center near the African coast (Fig. 1b) is associated with coastal upwelling by the fluctuating alongshore winds (Huang and Shukla 1997). It is interesting to note that the patterns similar to what we have shown in Figs. 7a and 8b, which are the model version of the STA mode, do not appear in the REOF modes of the thermal simulation. This implies that these model modes are produced by the dynamical air–sea interaction.

It is possible that the NTA and SSA patterns are formed by passive oceanic responses to the fluctuations of the surface heat flux induced by the atmospheric internal variability (Dommenget and Latif 2000). In this situation, the effect of the air–sea feedback is secondary. To test this hypothesis, we have conducted another experiment that has the same setting as the thermal run except that the SST field supplied to the AGCM over the Atlantic Ocean is replaced by a monthly climatology from the control run. Therefore, this run is actually an uncoupled OGCM simulation without any oceanic feedback to the atmosphere. The fluctuations of the surface heat flux, apart from its annual cycle, are caused by atmospheric internal variations.

Our examination of a 49-yr integration of this forced OGCM run shows that the surface heat flux from the atmospheric internal variability can generate large SST fluctuations in the ocean. However, the centers of the SSTA standard deviation from this forced run are near 30°S and 30°N in the central and western Atlantic Ocean. In comparison with the subtropics, the SST fluctuations are smaller in the tropical Atlantic within 10°S–10°N. The leading REOF patterns of the SST anomalies are significantly different from what we have seen in the coupled model and the observations. This seems to imply that thermodynamic air–sea feedback plays a role in generating the observed patterns of the tropical SST anomalies in the tropical ocean (Chang et al. 2001; HS).

To examine the influence of the model mean SST systematic errors on the major interannual SST patterns, especially the STA pattern, we have conducted a 100-yr simulation with a prescribed empirical surface heat flux correction term added to the regional coupled model. The heat flux correction term varies spatially but is constant in time. Its magnitude is based on the mean

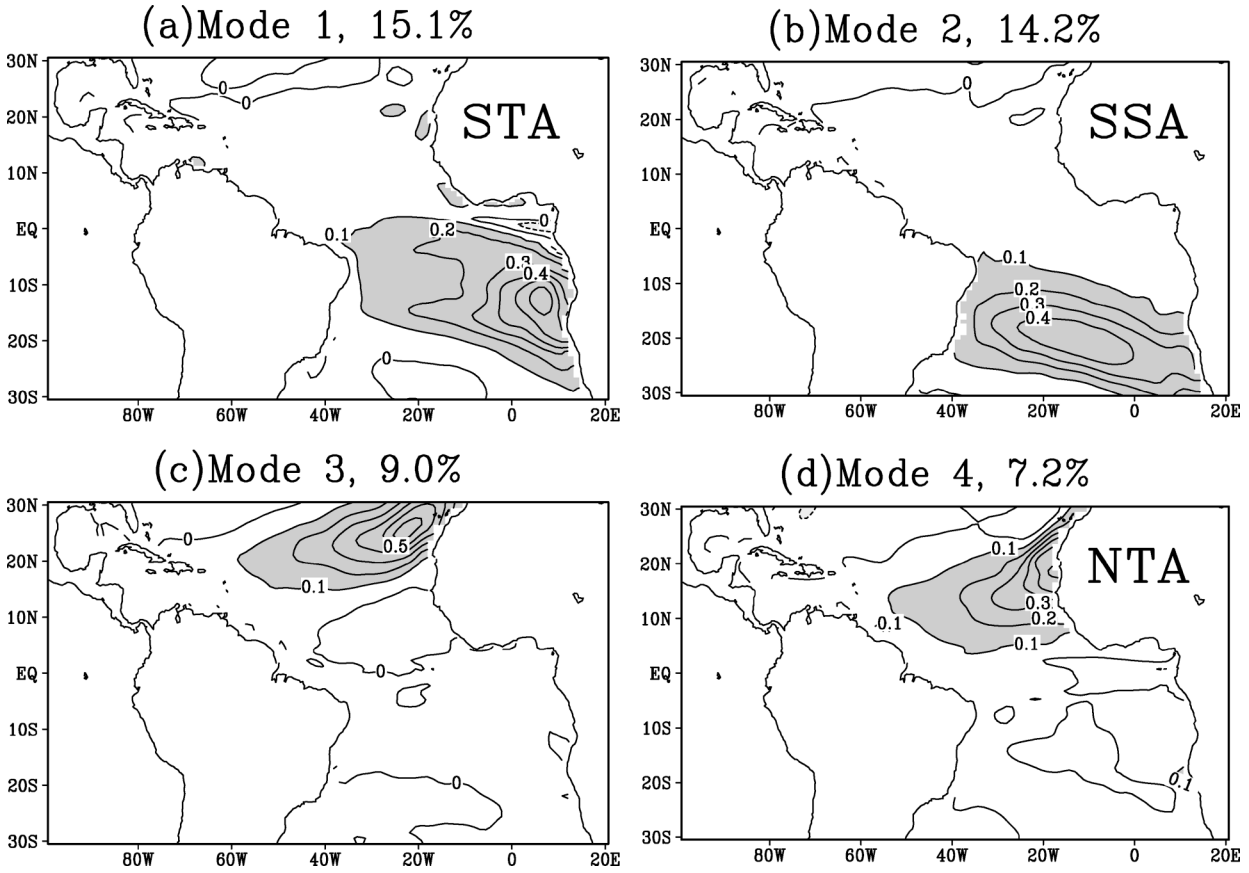

FIG. 11. The spatial patterns of the (a) first, (b) second, (c) third, and (d) fourth REOF modes of the seasonal mean SST anomalies from the flux-corrected experiment. The contour interval is 0.1°C. Regions with SST anomalies larger than 0.1°C are shaded. The corresponding time series of each mode is normalized by its standard deviation.

local SST error in the control simulation (Fig. 3e). This experiment is referred to as the ''flux corrected'' run hereafter. Due to the addition of this correction, the model annual mean SST errors in the Atlantic basin, especially those near the southeastern boundary, are significantly reduced. In this run, the mean SST errors are less than 1°C in most of the Atlantic domain within 20°S–20°N and smaller than 0.5°C in a large part of the domain. The annual cycle of the equatorial zonal wind stress is also improved in this flux-corrected run (not shown).

More importantly, with the improved mean zonal and meridional SST gradient, the STA pattern from the flux-corrected run becomes the first REOF mode and accounts for a higher fraction of the variance (15.1%) than in the control case (8.6%). The spatial structure of this mode is also more realistic, showing a stronger tendency to extend toward the equator (Fig. 11a). The equatorially trapped SST anomalies as shown in Fig. 8b are significantly weakened in this simulation (not shown). Moreover, the NTA and SSA patterns in the flux-corrected run (Figs. 11b,d) are the same as those in the control run (Figs. 7b,c). The SST anomalies in the northeastern part of the northern subtropical Atlantic Ocean are slightly enhanced due to the flux correction (Fig. 11c).

An integration of 80 yr of the regional coupled model is conducted while the fully coupled region is restricted within the tropical Atlantic Ocean between 30°S and 30°N with climatologies prescribed at the air–sea interface elsewhere. Referred to as the ''tropical'' run, this experiment tests whether the air–sea interactions in the North Atlantic have a significant influence on the tropical SST anomalies. We found that the leading spatial SST patterns derived from this run (Fig. 12) are not significantly different from those of the control run (Figs. 7 and 8). This suggests that the SST anomalies in the northern tropical Atlantic Ocean, such as the NTA pattern, are mainly generated locally by the fluctuations of the surface heat fluxes instead of propagating from the North Atlantic. The results also show that the midlatitude influences on the tropical Atlantic Ocean, such as the NAO effect, are mainly through the atmospheric disturbances propagating into the Tropics.

To check the potential influences of the artificial boundary placed at 30°S in the control run, we examined the leading REOF modes of the seasonally averaged

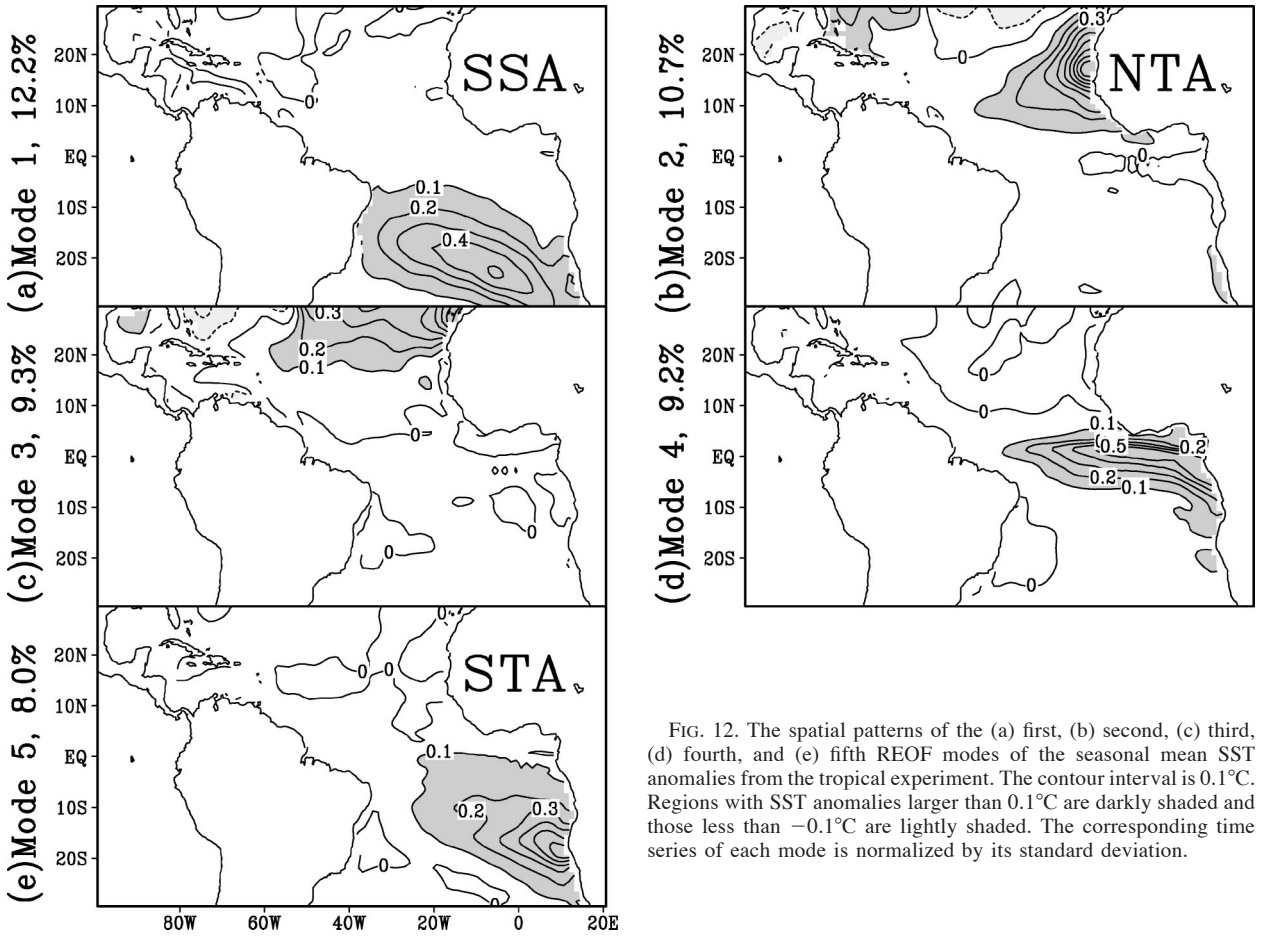

FIG. 12. The spatial patterns of the (a) first, (b) second, (c) third, (d) fourth, and (e) fifth REOF modes of the seasonal mean SST anomalies from the tropical experiment. The contour interval is 0.1°C. Regions with SST anomalies larger than 0.1°C are darkly shaded and those less than −0.1°C are lightly shaded. The corresponding time series of each mode is normalized by its standard deviation.

SST anomalies from a 300-yr simulation of the globally coupled version of the ocean–atmosphere GCM (Fig. 13). It is found that both the SSA (Fig. 13a) and NTA (Fig. 13d) patterns from the global coupled longer-term simulation are very similar to those shown in the control run. Therefore, it can be concluded that the influences of the artificial southern boundary in the control run are not detrimental to the simulated SSA pattern. One difference between the global and the control runs is that the global coupled simulation shows an enhanced equatorial mode around the eastern boundary (Fig. 13b). On the other hand, the mode that shows SST fluctuations near the southeastern boundary around 10°–15°S and was referred to as the model STA in the control run (Fig. 7a) is weaker (not shown). The enhanced equatorial mode in the globally coupled simulation is possibly associated with more active zonal wind fluctuations near the equator, which in turn are likely due to the allowed ENSO activity.

6. Summary

Tropical Atlantic variability is composed of a variety of SST fluctuations in the subtropics, Tropics, and the equatorial ocean. The fluctuations are generated by different mechanisms of regional air–sea feedback, passive oceanic responses to atmospheric forcing, and remote effects of major climate variations in other parts of the world. Understanding the roles played by these different processes and their interactions in producing the observed SST variability is a major issue in understanding the nature of the climate variations in this region and its potential predictability. In this study, we used a specially designed global ocean–atmosphere general circulation model to separate the effects of the regional air–sea coupling from remote forcing. In this model, the oceanic and atmospheric components are coupled with each other within the Atlantic Ocean between 30°S and 65°N, while both are forced by a prescribed mean annual cycle of SST and wind stress, respectively, over the rest of the uncoupled oceanic basin. This experimental design removes a major potential remote source of the tropical Atlantic variability, the Pacific El Niño–Southern Oscillation (ENSO).

An examination of a 110-yr simulation shows that the model reproduces the observed structures of the northern tropical Atlantic (NTA) and the southern subtropical Atlantic (SSA) patterns. Although the obser-

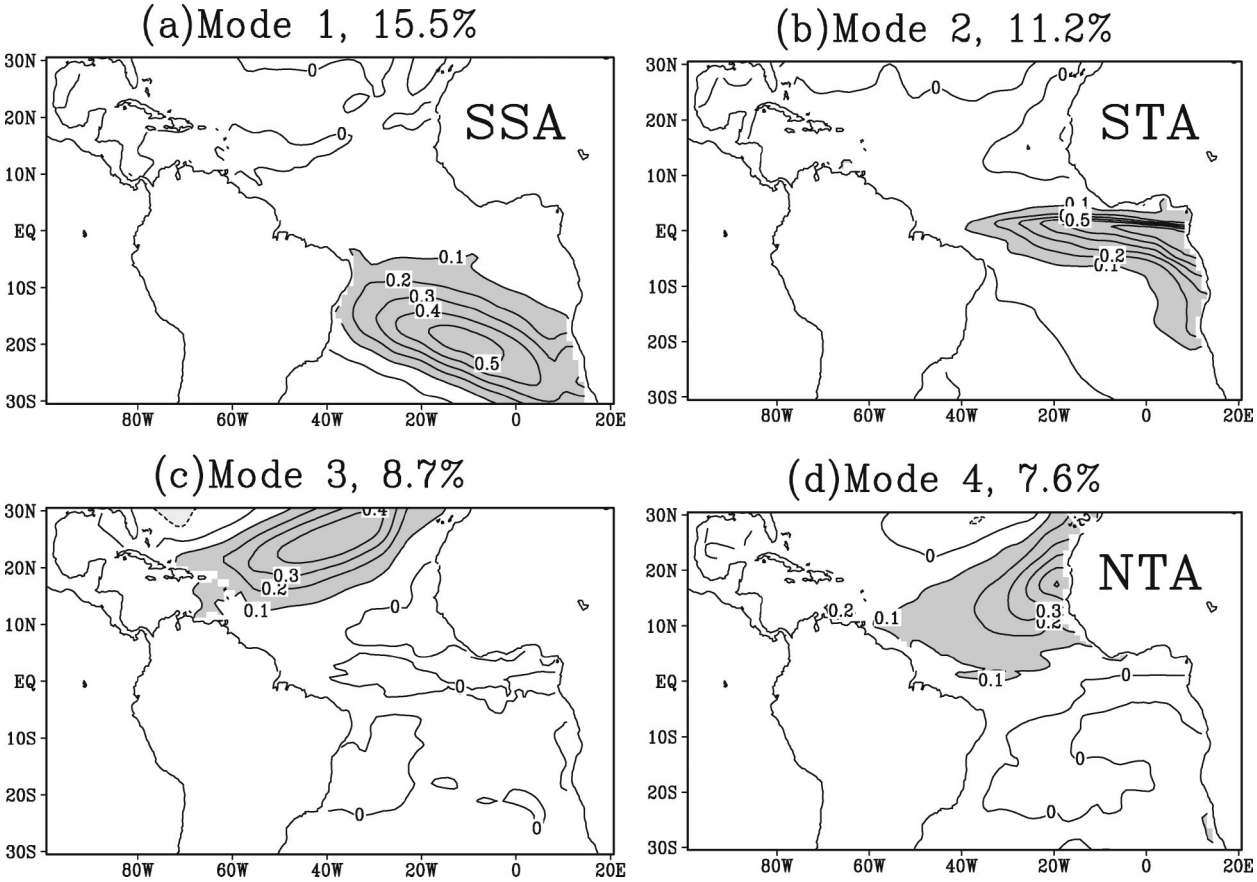

FIG. 13. The spatial patterns of the (a) first, (b) second, (c) third, and (d) fourth REOF modes of the seasonal mean SST anomalies from the globally coupled simulation. The contour interval is 0.1°C. Regions with SST anomalies larger than 0.1°C are shaded. The corresponding time series of each mode is normalized by its standard deviation.

vational record is only for 49 yr, it is reassuring that the 110-yr integration of the coupled model simulates the observed SSA and NTA patterns quite well. We have also carried out REOF analyses for three 50-yr segments of the 110-yr coupled run, and in each of the three segments these basic patterns are simulated. This implies that these patterns are mainly determined by ocean–atmosphere coupling within the Atlantic sector and oceanic responses to atmosphere internal noise. External forcing from outside the Atlantic basin is not crucial in determining their spatial structures.

The model also simulates some features of the southern tropical Atlantic (STA) pattern. However, there are serious flaws in this aspect. In particular, the observed STA pattern seems to split into two separate parts in the model, one stronger near the eastern boundary around 15°S and the other centered at the eastern equatorial ocean. The split of the STA pattern occurs in the model because, unlike the observations, the equatorial fluctuations and the thermocline changes near the southeastern part of the ocean are largely unconnected. It is reasonable to ask whether the lack of ENSO forcing and the possibly weaker effects from the southern extratropical ocean due to the regional coupling strategy are responsible for this problem in the model STA simulation. To answer these questions, we have examined a longer-term globally coupled run (Fig. 13) as well as an ensemble of eight experiments in which observed SST for 1950–98 is prescribed in the uncoupled region (not shown). We find that the equatorial SST fluctuations are enhanced in the globally coupled run and also in some of the hindcasts, likely related to the presence of the external influences. However, the split between the equatorial fluctuations and those near the southeastern boundary shows up in all of the simulations. We therefore conclude that the lack of ENSO and extratropical effects is not the primary reason for the model errors in the STA pattern.

We believe that the lack of connection between the equatorial and the southern tropical ocean is mainly caused by the model systematic bias, which produces weaker zonal winds near the equator and warmer SST to its south. Qualitatively similar patterns of the systematic errors are found in the globally coupled simulation and the hindcasts. This bias is linked to the seasonal shift of the intertropical convergence zone into

the Southern Ocean in boreal spring and the formation of warm surface water there. It is also likely contributed by the inadequate upwelling near the eastern boundary because of the weak alongshore winds there. The warm water formed to the south of the equator seems to block the equatorial fluctuations from propagating into the Southern Ocean effectively. Due to this systematic bias, this model did not simulate the tropical dynamical air–sea interactions adequately. Our flux-corrected simulation demonstrates that the STA mode can be significantly enhanced, and its pattern can be more realistic, if the warm SST bias to the south of the equator is reduced. Therefore, we believe that the errors in the mean state are the major obstacle preventing a realistic simulation of the SST fluctuations in the southeastern tropical Atlantic by this coupled model.

The pattern and magnitude of the systematic errors as demonstrated here are by no means unusual. In fact, this model (either the regionally or globally coupled version) is probably one of the better coupled models in simulating the mean SST in the equatorial Atlantic Ocean among present coupled GCMs. In particular, our model produces colder surface water residing in the eastern ocean with a zonal SST gradient along the equator from the western coast to around 10°W (Fig. 3a). Although this model gradient is weaker than observed, it is more consistent with the observations than some coupled simulations, which give zonal SST gradients opposite to the observations on the equator throughout the basin (Davey et al. 2000). We suspect that the models that cannot simulate the correct direction of the zonal SST gradient would have more difficulty in simulating the STA pattern. Therefore, the problem that we have demonstrated is a general one for state-of-the-art coupled ocean–atmosphere general circulation models.

Our sensitivity experiments demonstrate that both NTA and SSA patterns are mainly associated with the thermodynamic air–sea interactions while the STA pattern (or its model counterparts) is likely more closely associated with the dynamical response of the equatorial and tropical ocean to the surface wind forcing. Examining the composite events associated with these major patterns, HS showed that the atmospheric extratropical fluctuations play a significant role in causing the initial warmings in the northern and southern subtropical Atlantic that evolve into major NTA and SSA episodes. These results are largely consistent with those derived by Dommenget and Latif (2000). Examining annual mean SST data from several globally coupled ocean–atmosphere general circulation models (CGCMs), they have pointed out that the surface heat flux fluctuations associated with the fluctuations of subtropical anticyclones are a major mechanism causing the tropical Atlantic SST variability. In fact, the two leading REOF modes of our model simulation, the SSA (Fig. 7c) and NTA (Fig. 7b), are very similar to the two leading modes from the models Dommenget and Latif (2000) have described (see their Fig. 6).

However, our results seem to differ from Dommenget and Latif's (2000) conclusion that major tropical Atlantic SST fluctuations passively respond to local atmospheric forcing. Our preliminary analysis of an uncoupled ocean simulation with surface heat flux from an atmospheric model output under climatological SST forcing shows quite different distributions of the standard deviation and leading modes of the SST anomalies from those of both observed and coupled model distributions. Since the latter two are more similar to each other, this seems to imply that air–sea interactions do play some role in forming the observed NTA and SSA patterns. This is consistent with the responses of the tropical ocean–atmosphere to the subtropical anomalies shown by HS. As we have mentioned above, one of the two leading REOF SST modes from all coupled models reported in Dommenget and Latif (2000) is similar to the observed SSA pattern shown in this study. However, the observed southern Atlantic mode that they compare with (their Fig. 4a), in our opinion, has some features of the STA mode identified here (Fig. 1a). Our present analysis tries to distinguish between the characteristics of the STA and SSA patterns in the southern tropical and subtropical Atlantic Ocean based on their different mechanisms.

At this stage, we cannot conclude that the southern tropical Atlantic SST variability is mainly caused by heat flux forcing from the subtropics, while air–sea feedback and ocean dynamics have little effect. In fact, based on our analysis above, the contribution of regional air–sea coupling and oceanic dynamics is likely significant for the STA pattern, which, in reality, accounts for a much larger portion of the total variance than the SSA mode does. The obstacle that prevents a further analysis of the mechanisms of the STA pattern is the inadequacy of the present coupled models in simulating this mode realistically. As we have mentioned before, it is possible that, in many present coupled models, the dynamic oceanic fluctuations represented by the STA mode are severely underestimated.

In a previous study using an earlier version of the regional coupled model forced with observed SSTs for the period 1950–98 over the uncoupled domain, Huang et al. (2002b) found significant ENSO influence on the NTA, which is similar to the observed ENSO–NTA relationship (Enfield and Mayer 1997). The present experiment suggests that the spatial pattern of the NTA is mainly determined by ocean–atmosphere coupling within the Atlantic Ocean. The effect of ENSO may be primarily to modulate the temporal evolution of the NTA through influencing atmospheric planetary waves influencing the Atlantic basin. More recently, a more comprehensive study was presented by Huang (2003), which examined an ensemble of eight regional coupled runs with the observed SST forcing for 1950–98. Apart from the NTA pattern, it is found that ENSO may also have some influence on the STA and SSA modes, as shown in the ensemble.

Acknowledgments. This study is supported by grants (NA96GP0446 and NA169PI570) from National Oceanic and Atmospheric Administration's CLIVAR Atlantic Program. We would like to thank Dr. B. Kirtman for helping us to develop the coupled model and Mr. Z. Pan for programming work. We would also like to thank Drs. Q. Wu and V. Krishnamurthy for discussions on the application of spectral analysis, Drs. B. Klinger and D. Straus for editing and commenting on an earlier version of the manuscript, and Professor M. Latif and two anonymous reviewers for making many valuable suggestions for the revision of this paper. Some computational resources were provided by the Scientific Computing Division, National Center for Atmospheric Research.

REFERENCES

Bretherton, C. S., M. Widmann, V. Dymnikov, J. M. Wallace, and I. Bladé, 1999: The effective number of spatial degrees of freedom of a time-varying field. *J. Climate,* **12,** 1990–2009.

Cabosnarvaez, W., F. A. Garcia, and M. J. Ortizbevia, 2002: Generation of equatorial Atlantic warm and cold events in a coupled general circulation model simulation. *Tellus,* **54A,** 426–438.

Carton, J. A., and B. Huang, 1994: Warm events in the tropical Atlantic. *J. Phys. Oceanogr.,* **24,** 888–903.

Chang, P., L. Ji, and H. Li, 1997: A decadal climate variation in the tropical Atlantic Ocean from thermodynamic air–sea interactions. *Nature,* **385,** 516–518.

——, ——, and R. Saravanan, 2001: A hybrid coupled model study of tropical Atlantic variability. *J. Climate,* **14,** 361–390.

Curtis, S., and S. Hastenrath, 1995: Forcing of anomalous surface temperature evolution in the tropical Atlantic during Pacific warm events. *J. Geophys. Res.,* **100** (C8), 15 835–15 847.

Czaja, A., and C. Frankignoul, 2002: Observed impact of Atlantic SST anomalies on the North Atlantic Oscillation. *J. Climate,* **15,** 3280–3290.

——, P. van der Vaart, and J. Marshall, 2002: A diagnostic study of the role of remote forcing in tropical Atlantic variability. *J. Climate,* **15,** 3280–3290.

da Silva, A. M., C. C. Young-Molling, and S. Levitus, 1994: *Algorithms and Procedures.* Vol. 1, *Atlas of Surface Marine Data 1994,* NOAA Atlas NESDIS 6, 83 pp.

Davey, M., M. Huddleston, and K. R. Sperber, 2000: STOIC: A study of coupled model climatology and variability in tropical ocean regions. *CLIVAR Exchanges,* Vol. 5, No. 3, International CLIVAR Project Office, Southampton, United Kingdom, 21–23.

Davies, R., 1982: Documentation of the solar radiation parameterization in the GLAS climate model. NASA Tech. Memo. 83961, 57 pp.

Delecluse, P., J. Servain, C. Levy, K. Arpe, and L. Bengtsson, 1994: On the connection between the 1984 Atlantic warm event and the 1982–1983 ENSO. *Tellus,* **46A,** 448–464.

DeWitt, 1996: The effect of the cumulus convection scheme on the climate of the COLA general circulation model. COLA Tech. Rep. 27, 58 pp.

Dommenget, D., and M. Latif, 2000: Interannual and decadal variability in the tropical Atlantic. *J. Climate,* **13,** 777–792.

Enfield, D. B., 1996: Relationships of inter-American rainfall to tropical Atlantic and Pacific SST variability. *Geophys. Res. Lett.,* **23,** 3305–3308.

——, and D. A. Mayer, 1997: Tropical Atlantic sea surface temperature variability and its relation to El Niño–Southern Oscillation. *J. Geophys. Res.,* **102,** 929–945.

——, and E. J. Alfaro, 1999: The dependence of Caribbean rainfall on the interaction of the tropical Atlantic and Pacific Oceans. *J. Climate,* **12,** 2093–2103.

——, A. M. Mestas-Nuñez, D. A. Mayer, and L. Cid-Serrano, 1999: How ubiquitous is the dipole relationship in tropical Atlantic sea surface temperature? *J. Geophys. Res.,* **104,** 7841–7848.

Folland, C., T. Palmer, and D. Parker, 1986: Sahel rainfall and worldwide sea surface temperatures. *Nature,* **320,** 602–606.

Fraedrich, K., C. Ziehmann, and F. Sielmann, 1995: Estimates of spatial degree of freedom. *J. Climate,* **8,** 361–369.

Giannini, A., Y. Kushnir, and M. A. Cane, 2000: Interannual variability of Caribbean rainfall, ENSO, and the Atlantic Ocean. *J. Climate,* **13,** 297–311.

Häkkinen, S., and K. C. Mo, 2002: The low-frequency variability of the tropical Atlantic Ocean. *J. Climate,* **15,** 237–250.

Harshvardhan, R. Davis, D. A. Randall, and T. G. Corsetti, 1987: A fast radiation parameterization for general circulation models. *J. Geophys. Res.,* **92,** 1009–1016.

Harzallah, A., J. O. Rocha De Aragao, and R. Sadourny, 1996: Interannual rainfall variability in northeast Brazil: Observation and model simulation. *Int. J. Climatol.,* **16,** 861–878.

Hastenrath, S., 1976: Variations in low-latitude circulation and extreme climatic events in the tropical Americas. *J. Atmos. Sci.,* **33,** 202–215.

——, 1984: Interannual variability and annual cycle: Mechanisms of circulation and climate in the tropical Atlantic sector. *Mon. Wea. Rev.,* **112,** 1097–1107.

——, 1990: Prediction of northeast Brazil rainfall anomalies. *J. Climate,* **3,** 893–904.

——, and L. Heller, 1977: Dynamics of climate hazards in Northeast Brazil. *Quart. J. Roy. Meteor. Soc.,* **103,** 77–92.

Hirst, A., and S. Hastenrath, 1983: Atmosphere–ocean mechanisms of climate anomalies in the Angola–tropical Atlantic sector. *J. Phys. Oceanogr.,* **13,** 1146–1157.

Horel, J. D., V. E. Kousky, and M. T. Kagaro, 1986: Atmospheric conditions in the tropical Atlantic during 1983 and 1984. *Nature,* **322,** 243–245.

Houghton, R. W., and Y. Tourre, 1992: Characteristics of low frequency sea surface temperature fluctuations in the tropical Atlantic. *J. Climate,* **5,** 765–771.

Huang, B., 2003: Remotely forced variability in the tropical Atlantic Ocean. *Climate Dyn.,* in press.

——, and E. K. Schneider, 1995: The response of an ocean general circulation model to surface wind stress produced by an atmospheric general circulation model. *Mon. Wea. Rev.,* **123,** 3059–3085.

——, and J. Shukla, 1997: An examination of AGCM simulated surface wind stress and low-level winds over the tropical Pacific Ocean. *Mon. Wea. Rev.,* **125,** 985–998.

——, P. S. Schopf, and J. Shukla, 2002a: Coupled ocean–atmosphere variability in the tropical Atlantic Ocean. *CLIVAR Exchanges,* Vol. 7, No. 3/4, International CLIVAR Project Office, Southampton, United Kingdom, 24–27.

——, ——, and ——, 2002b: The ENSO effect on the tropical Atlantic variability: A regionally coupled model study. *Geophys. Res. Lett.,* **29,** 2039, doi:10:1029/2002GL014872.

Jury, M. R., H. Mulenga, and H. Rautenbach, 2000: Tropical Atlantic variability and Indo–Pacific ENSO: Statistical analysis and numerical simulation. *Global Atmos. Ocean Syst.,* **7,** 107–124.

Kalnay, E., and Coauthors, 1996: The NCEP/NCAR 40-Year Reanalysis Project. *Bull. Amer. Meteor. Soc.,* **77,** 437–471.

Kiehl, J. T., J. J. Hack, and B. P. Briegleb, 1994: The simulated Earth radiation budget of the National Center for Atmospheric Research Community Climate Model CCM2 and comparisons with the Earth Radiation Budget Experiment (ERBE). *J. Geophys. Res.,* **99,** 20 815–20 827.

Lacis, A. A., and J. E. Hansen, 1974: A parameterization for the absorption of solar radiation in the earth's atmosphere. *J. Atmos. Sci.,* **31,** 118–133.

Lamb, P. J., 1978a: Case studies of tropical Atlantic surface circu-

lation patterns during recent sub-Sahara weather anomalies: 1967 and 1968. *Mon. Wea. Rev.,* **106,** 482–491.
——, 1978b: Large-scale tropical Atlantic surface circulation patterns associated with subsuharan weather anomalies. *Tellus,* **30,** 240–251.
——, and R. A. Peppler, 1991: West Africa. *Teleconnections Linking Worldwide Climate Anomalies,* M. Glantz, R. Katz, and N. Nicholls, Eds., Cambridge University Press, 121–189.
Latif, M., and T. P. Barnett, 1995: Interaction of the tropical oceans. *J. Climate,* **8,** 952–964.
——, and A. Grötzner, 2000: The equatorial Atlantic oscillation and its response to ENSO. *Climate Dyn.,* **16,** 213–218.
Liu, T., and X. Xie, 2002: Double intertropical convergence zones—a new look using scatterometer. *Geophys. Res. Lett.,* **29,** 2072, doi:10.1029/2002GL015431.
Lough, J. M., 1986: Tropical Atlantic sea surface temperatures and rainfall variations in Subsaharan Africa. *Mon. Wea. Rev.,* **114,** 561–570.
Mechoso, C. R., and Coauthors, 1995: The seasonal cycle over the tropical Pacific in coupled ocean–atmosphere general circulation models. *Mon. Wea. Rev.,* **123,** 2825–2838.
Meehl, G. A., and J. M. Arblaster, 1998: The Asian–Australian monsoon and El Niño–Southern Oscillation in the NCAR Climate System Model. *J. Climate,* **11,** 1356–1385.
Mehta, V., 1998: Variability of the tropical ocean surface temperatures at decadal–multidecadal timescales. Part I: The Atlantic Ocean. *J. Climate,* **11,** 2351–2375.
Mellor, G. L., and T. Yamada, 1982: Development of a turbulence closure model for geophysical fluid problems. *Rev. Geophys. Space Phys.,* **20,** 851–875.
Mo, K.-C., and S. Häkkinen, 2001: Interannual variability in the tropical Atlantic and linkages to the Pacific. *J. Climate,* **14,** 2740–2762.
Moorhi, S., and M. J. Suarez, 1992: Relaxed Arakawa–Schubert: A parameterization of moist convection for general circulation models. *Mon. Wea. Rev.,* **120,** 978–1002.
Moura, A. D., and J. Shukla, 1981: On the dynamics of droughts in northeast Brazil: Observations, theory and numerical experiments with a general circulation model. *J. Atmos. Sci.,* **38,** 2653–2675.
Neelin, J. D., and Coauthors, 1992: Tropical air–sea interaction in general circulation models. *Climate Dyn.,* **7,** 73–104.
Niiler, P. P., and E. B. Kraus, 1977: One-dimentional models of the upper ocean. *Modelling and Prediction of the Upper Layers of the Ocean,* E. B. Kraus, Ed., Pergamon, 143–172.
Nobre, P., and J. Shukla, 1996: Variations of sea surface temperature, wind stress, and rainfall over the tropical Atlantic and South America. *J. Climate,* **9,** 2464–2479.
Pacanowski, R. C., and S. G. H. Philander, 1981: Parameterization of vertical mixing in numerical models of tropical oceans. *J. Phys. Oceanogr.,* **11,** 1443–1451.
Palmer, T. N., G. J. Shutts, and R. Swinbank, 1986: Alleviation of a systematic westerly bias in general circulation and numerical weather prediction model through an orographic gravity wave parameterization. *Quart. J. Roy. Meteor. Soc.,* **112,** 1001–1039.
Robertson, A. W., and C. R. Mechoso, 2000: Interannual and interdecadal variability of the South Atlantic convergence zone. *Mon. Wea. Rev.,* **128,** 2947–2957.
Roeckner, E., J. M. Oberhuber, A. Bacher, M. Cristoph, and I. Kirchner, 1995: ENSO variability and atmospheric response in a global coupled ocean-atmosphere GCM. Max-Planck-Institut für Meteorology Rep. 178, 33 pp.
Roy, C., and C. Reason, 2001: ENSO related modulation of coastal upwelling in the eastern Atlantic. *Progress in Oceanography,* Vol. 49, Pergamon, 245–255.
Saravanan, R., and P. Chang, 2000: Interaction between tropical Atlantic variability and El Niño–Southern Oscillation. *J. Climate,* **13,** 2177–2194.
Schneider, E. K., Z. Zhu, B. S. Giese, B. Huang, B. P. Kirtman, J. Shukla, and J. A. Carton, 1997: Annual cycle and ENSO in a coupled ocean–atmosphere model. *Mon. Wea. Rev.,* **125,** 680–702.
——, B. P. Kirtman, Y. Fan, and Z. Zhu, 2001: Retrospective ENSO forecasts: The effect of ocean resolution. COLA Tech. Rep. 109, 27 pp.
Schopf, P. S., and A. Loughe, 1995: A reduced-gravity isopycnal ocean model: Hindcasts of El Niño. *Mon. Wea. Rev.,* **123,** 2839–2863.
Shapiro, R., 1970: Smoothing, filtering and boundary effects. *Rev. Geophys. Space Phys.,* **8,** 359–387.
Smith, T. M., R. W. Reynolds, R. E. Livezey, and D. C. Stokes, 1996: Reconstruction of historical sea surface temperatures using empirical orthogonal functions. *J. Climate,* **9,** 1403–1420.
Tanimoto, Y., and S.-P. Xie, 1999: Ocean–atmosphere variability over the pan-Atlantic basin. *J. Meteor. Soc. Japan,* **77,** 31–46.
Tiedtke, M., 1984: The effect of penetrative cumulus convection on the large-scale flow in a general circulation model. *Beitr. Phys. Atmos.,* **57,** 216–239.
Tourre, Y., M. B. Rajagopalan, and Y. Kushnir, 1999: Dominant patterns of climate variability in the Atlantic Ocean region during the last 136 years. *J. Climate,* **12,** 2285–2299.
Venegas, S. A., L. A. Mysak, and D. Straub, 1997: Atmosphere–ocean coupled variability in the South Atlantic. *J. Climate,* **10,** 2904–2920.
Wagner, R. G., and A. da Silva, 1994: Surface conditions associated with anomalous rainfall in the Guinea coastal region. *Int. J. Climatol.,* **14,** 179–199.
Ward, N., and C. K. Folland, 1991: Prediction of seasonal rainfall in the north Nordeste of Brazil using eigenvectors of sea surface temperature. *Int. J. Climatol.,* **11,** 711–743.
Williamson, D. L., J. T. Kiehl, and J. J. Hack, 1995: Climate sensitivity of the NCAR Community Climate Model (CCM2) to horizontal resolution. *Climate Dyn.,* **11,** 377–398.
Xie, S.-P., 1999: A dynamic ocean–atmosphere model of the tropical Atlantic decadal variability. *J. Climate,* **12,** 64–70.
Yu, Z., and P. S. Schopf, 1997: Vertical eddy mixing in the tropical upper ocean: Its influence on zonal currents. *J. Phys. Oceanogr.,* **27,** 1447–1458.
Zebiak, S. E., 1993: Air–sea interaction in the equatorial Atlantic region. *J. Climate,* **6,** 1567–1586.
——, and M. A. Cane, 1987: A model El Niño–Southern Oscillation. *Mon. Wea. Rev.,* **115,** 2262–2278.